

ON-LINE MEASUREMENT OF CRYSTALLIZATION DYNAMICS AND  
KINETICS USING A LASER PARTICLE-SIZE ANALYZER

by

Chi-Chu David Low

---

A Thesis Submitted to the Faculty of the  
DEPARTMENT OF CHEMICAL ENGINEERING  
In Partial Fulfillment of the Requirements  
For the Degree of  
MASTER OF SCIENCE  
In the Graduate College  
THE UNIVERSITY OF ARIZONA

1 9 8 0

STATEMENT BY AUTHOR

This thesis has been submitted in partial fulfillment of requirements for an advanced degree at The University of Arizona and is deposited in the University Library to be made available to borrowers under rules of the Library.

Brief quotations from this thesis are allowable without special permission, provided that accurate acknowledgement of source is made. Requests for permission for extended quotation from or reproduction of this manuscript in whole or in part may be granted by the head of the major department or the Dean of the Graduate College when in his judgment the proposed use of the material is in the interests of scholarship. In all other instances, however, permission must be obtained from the author.

SIGNED:

Chi-chu David Low

APPROVAL BY THESIS DIRECTOR

This thesis has been approved on the date shown below:

A. D. Randolph

A. D. RANDOLPH

Professor of Chemical Engineering

8/21/80

Date

## ACKNOWLEDGMENTS

I express my deepest gratitude to Dr. Alan D. Randolph, my advisor, for his continued guidance and encouragement throughout this study and my graduate program. Appreciation is extended to Dr. E. T. White of The University of Queensland for his valuable advice and suggestions. I also thank the other faculty members of the Department of Chemical Engineering at The University of Arizona for their help during my stay.

My sincere thanks to Dr. James W. White, James Colburn, and Roger Montgomery for setting up the on-line computer work. The zone sensing analysis performed by Mr. H. E. Jones is also appreciated.

I am thankful to Mr. Sal Gonzales of the College of Mines Electronics Shop and Mr. Dick Van Reeth of the Machine Shop for their assistance in many things crucial for this study.

Finally, I am grateful to the National Science Foundation for financial support through Grant ENG-77-23925.

## TABLE OF CONTENTS

	Page
LIST OF ILLUSTRATIONS . . . . .	vi
LIST OF TABLES . . . . .	viii
ABSTRACT . . . . .	ix
1. INTRODUCTION . . . . .	1
2. LITERATURE REVIEW . . . . .	4
Dynamics and Control . . . . .	4
Particle Size Analyzer . . . . .	9
Laser Light Scattering Techniques . . . . .	9
Zone-Sensing Techniques . . . . .	11
3. CRYSTALLIZER THEORY . . . . .	13
Process Models . . . . .	13
Interrelationship between $B^\circ$ , $G$ , $s$ , and CSD . . . . .	15
Nucleation Kinetics . . . . .	17
Control Algorithm . . . . .	18
4. EXPERIMENTAL . . . . .	20
Description of Equipment . . . . .	20
Feed Tank . . . . .	20
Crystallizer and Fines Trap . . . . .	22
Crystallizer Cooling System . . . . .	23
Fines Destruction System . . . . .	23
Sampling System . . . . .	23
Particle-Sizer and Analysis System . . . . .	25
Experimental Procedure . . . . .	29
Instrument Tests . . . . .	29
Operation of Equipment . . . . .	31
Start-Up . . . . .	32
Shut-Down . . . . .	33
5. EXPERIMENTAL RUNS . . . . .	34
Experimental Conditions . . . . .	34
Results . . . . .	35

TABLE OF CONTENTS--Continued

	Page
6. DISCUSSION AND ANALYSIS OF RESULTS . . . . .	49
Crystallizer Responses . . . . .	49
Response at Steady State . . . . .	49
Response to Agitation Rate Decrease . . . . .	49
Response to Agitation Rate Increase . . . . .	52
Response to Fines Rate Increase . . . . .	52
Response to Fines Rate Decrease . . . . .	54
Response to Feed Rate Change . . . . .	55
Response to Temperature Upset . . . . .	56
Instrument Performance . . . . .	57
Nucleation Kinetics Model . . . . .	60
7. SUMMARY AND CONCLUSIONS . . . . .	64
APPENDIX A: ON-LINE DATA REDUCTION . . . . .	66
APPENDIX B: CALIBRATION AND INSTALLATION OF LIGHT SCATTERING INSTRUMENT . . . . .	72
APPENDIX C: EXPERIMENTAL DATA . . . . .	79
NOMENCLATURE . . . . .	97
LIST OF REFERENCES . . . . .	99

## LIST OF ILLUSTRATIONS

Figure	Page
1. Interrelationship between Nucleation Rate, Growth Rate, Supersaturation, and Crystal-Size Distribution . . . . .	16
2. Schematic Diagram of Experimental Equipment . . . . .	21
3. Schematic Drawing of Fines Trap Device . . . . .	24
4. Sample Line Flow Diagram . . . . .	26
5. Light Scattering Particle-Size Analyzer . . . . .	27
6. Information Flow Diagram . . . . .	30
7. Response at Steady State, Run 5/22/79/SS-1 . . . . .	37
8. Response to an Agitator Speed Decrease, Run 6/13/79/RP-2 . . . . .	38
9. Response to an Agitator Speed Increase, Run 7/31/79/RP-3 . . . . .	39
10. Response to an Agitator Speed Increase, Run 9/5/79/RP-4 . . . . .	40
11. Response to a Fines Dissolution Rate Increase, Run 5/17/79/QF-1 . . . . .	41
12. Response to a Fines Dissolution Rate Decrease, Run 6/26/79/QF-3 . . . . .	42
13. Response to a Fines Dissolution Rate Decrease, Run 8/21/79/QF-4 . . . . .	43
14. Response to a Feed Rate Increase, Run 5/15/79/QI-1 . . . . .	45
15. Response to a Feed Rate Decrease, Run 8/2/79/QI-3 . . . . .	46
16. Response to a Feed Rate Increase, Run 8/29/79/QI-4 . . . . .	47
17. Response to a Temperature Upset, Run 6/20/79/QF-2 . . . . .	48
18. Distribution of Surface Area in Crystal Product Size Distribution . . . . .	51

LIST OF ILLUSTRATIONS--Continued

Figure	Page
19. Nucleation Rate Correlated with Growth Rate and Slurry Density . . . . .	63

LIST OF TABLES

Table		Page
1.	Variables Studied and Operating Ranges . . . . .	36
2.	Experimental Operating Conditions . . . . .	36
3.	Summary of Experimental Steady-State Values Used in the Determination of Kinetic Parameters . . . . .	61

## ABSTRACT

An on-line technique was developed to determine crystal growth rate and nucleation rate on a continuous basis which would facilitate on-line control of the product-size distribution in crystallization processes. This was done by integrating a light-scattering, particle-size analyzer associated with a minicomputer into the fines recirculation loop of a continuous crystallizer.

Several tests were performed to test the instrument accuracy and reproducibility. A series of experiments was performed with the particle-size analyzer on-line to track specific crystallizer dynamic responses to known upsets. The instrument performed well, giving the responses expected for such perturbations.

A nucleation kinetics model of the potassium chloride-water system was experimentally determined. The model is in agreement with theoretical considerations.

## CHAPTER 1

### INTRODUCTION

Crystal-size distribution (CSD) is one of the key properties determining the acceptability of product from an operating crystallizer. Crystal-size distribution also is one of the most difficult to predict and least understood properties of crystallization processes.

Numerous studies on CSD dynamics have been made since the early 1960's. There are two types of dynamic modes that a crystallizer may experience; namely, transients and instability. CSD transients are excursions in time caused by outside disturbances such as fluctuations in temperature, flow rate, or stirrer rate. CSD instability is sustained internal limit-cycles in particle size caused by the interaction of system kinetics with process configuration (the size-dependent, residence-time distribution in the system) which are self-perpetuated. Much effort has been spent in controlling continuous crystallizers to maintain a desired CSD, i.e., reducing CSD transients and eliminating CSD instability. However, this still remains a long-standing and unsolved problem. Randolph (In press) has reviewed the state of the art, describing the problems involved and the methods used to model the dynamic behavior of crystallizers. Little has been done in the area of practical control of CSD.

To implement any CSD control algorithm requires the development of on-line particle measurement and data reduction technology. This involves measuring the crystal-size distribution to predict crystal growth rate ( $G$ ) and nucleation rate ( $B^\circ$ ).

A method of on-line analysis of this type is described by Rovang (1978). This was accomplished by integrating a Coulter Counter<sup>R</sup> into the fines loop of a laboratory KCl crystallizer. The size distribution of the fines followed the predicted exponential relation

$$n = \frac{B^\circ}{G} \exp(-L/G\tau) \quad [1]$$

and values of  $B^\circ$  and  $G$  were found by regression of the size data using an on-line, real-time minicomputer. The dynamic behavior of the crystallizer was tracked using this apparatus.

Because of orifice blocking problems, it is unlikely that a small orifice zone sensing instrument would be practical in an industrial environment. There are further problems due to electrical noise caused by the flowing conducting fluid (Rovang, 1978), although with careful design these problems might be avoided.

At the present time, on-line particle-size analysis techniques utilizing forward low-angle laser light scattering instruments are being developed. One such instrument is the Leeds and Northrup "Microtrac" particle analyzer. This instrument allows unrestricted sample flow up to 30 gal/min, and is designed for industrial sizing applications. Measurement of particles in the size range of 2 to 170  $\mu\text{m}$  at concentrations up to about 0.1% by volume is feasible with this instrument.

These conditions are a good match to conditions in the fines dissolution loop of a KCl crystallizer, and possibly in fines loops for many crystallizers. The basic nature of a fines dissolution loop automatically accomplishes the extensive sample conditioning that would otherwise be necessary.

The present work describes use of the Microtract instrument as an on-line particle-size analyzer in the fines loop of a KCl crystallizer. The crystallizer is the same as that used by Rovang (1978) and the on-line computation is carried out with the same minicomputer system. Specific goals of this study were as follows:

1. To show the feasibility of nucleation and growth rate measurement techniques using an on-line laser particle-size analyzer with associated minicomputer.
2. To demonstrate specific crystallizer dynamic responses to known upsets in a well-documented, bench-scale KCl crystallizer.
3. To demonstrate the feasibility of parameter estimation in a model for the system's nucleation/growth rate kinetics, utilizing on-line nucleation and growth rate data.

## CHAPTER 2

### LITERATURE REVIEW

The dynamics of crystal-size distribution (CSD) have been studied since the early 1960's. The development of crystallization technology now has moved to the area of control of such dynamic crystallizers. Whatever the control algorithm to be used, a necessary requirement is for an on-line instrument to measure the state of the system.

#### Dynamics and Control

CSD cycling problems in industrial crystallizers have long been recognized in both Class I (variable yield) and Class II (high yield) systems. Some industrial examples of cycling in Class I crystallizers were given by Bennett (1962). Robinson and Roberts (1957) described long-term transients and instability in an industrial ammonium sulfate crystallizer.

Consider the theoretical treatment of the Class I (variable yield) system. Sherwin, Shinnar, and Katz (1967) studied the dynamic behavior of an ideal mixed suspension, mixed product removal (MSMPR) Class I crystallizer. They found that correct feeding of the seed would stabilize the system and increase particle size. Of course, if seed is added externally, the feedback between supersaturation, crystal area, and nucleation is broken and the system is stabilized. Sherwin, Shinnar, and Katz (1969) were the first to notice the strong effect of

product classification on CSD stability. They assumed no product draw-off greater than the cut size  $L_p$ , and that as soon as a particle grew to the cut size  $L_p$  the particle was removed instantaneously. This study demonstrated that extreme classification could lower the nucleation stability limit to the range of realistic nucleation kinetics, thus possibly explaining CSD instability.

Hulburt and Stefango (1969) investigated a crystallizer with double draw-off, i.e., a mixed product underflow and a fines overflow (clear liquor advance). Such crystallizers increase particle size and solids content by increasing particle residence times. However, even with the lowest calculated stability limit, this model could not predict instability for reasonable nucleation/growth kinetic values.

Lei, Shinnar, and Katz (1971a) described a stability analysis of a continuous crystallizer with a fines trap. They concluded that stability was initially enhanced by using a fines trap, but was ultimately decreased as the fines removal rate was increased.

Some literature is also concerned with dynamics and stability of Class II systems. Randolph (1964) reported the first results pertaining to the stability of Class II MSMPR crystallizers. Stability was quantified such that if the slope of the log nucleation rate versus log growth rate plot were less than 21, stability would be guaranteed.

Nyvelt and Mullin (1970) presented a dynamic mathematical model for a Class II crystallizer. With this model they explain the periodic behavior of a continuous crystallizer. Nuttall (1971) developed the Mark III computer simulation to numerically model CSD dynamics using the

distributed dynamic population balance. However, this direct numerical simulation of the distributed CSD equations required large computer run times.

Randolph, Beer, and Keener (1973) studied the stability of CSD for the R-Z model of a Class II classified crystallizer with fines removal using spectral analysis of the linearized population balance. Their study showed that the most influential parameters leading to CSD instability were fines destruction and product classification. The stability limit (log derivative of  $B^\circ$  vs.  $G$ ) is lowered to the range of from one to five for such complex systems (versus 21 for the MSMPR crystallizer).

The transient behavior of Class II crystallizers with product classification was modeled by Shields (1976). He concluded that "an unsteady state model is a necessary reinforcement for steady state mathematical models for design, operating or troubleshooting exercises on crystallization plants" (Shields, 1976, p. 10). Leer, Konig, and De Jong (1976) studied the characteristic equation of the R-Z model derived by Randolph et al. (1973) to determine the location of the poles in the complex plane as a function of the dimensionless parameters of the model. Their analysis showed the effect that each pole has on stability and frequency of the model state variables. From the location of all the poles, the stability limits can be quantified.

Randolph, Beckman, and Kraljevich (1977) demonstrated, both experimentally and theoretically, that low-order cycling behavior was induced principally by product classification. Sustained limit-cycle

behavior in CSD was generated in a bench-scale, potassium chloride crystallizer with fines destruction, product classification, and clear liquor advance. Beckman (1976) developed a computer simulation of the complex crystallizer and successfully predicted dynamic CSD behavior.

Analytical studies of the dynamic behavior of crystallizers have moved crystallization theory towards the field of CSD control. However, studies and applications of CSD control have been limited due to the lack of on-line instrument techniques.

Han (1967) presented a feedforward control scheme to improve the dynamics of an uncontrolled Class I MSMPR crystallizer. Supersaturation in the crystallizer was controlled by applying feed rate as the manipulated variable with feed concentration as the input disturbance. He concluded that the system was well-controlled when feedforward control was applied in a stable region, i.e., where sustained CSD cycles did not occur. However, his control system failed to eliminate sustained limit-cycle behavior when the crystallizer was operated in an unstable region.

Timm and Gupta (1970) analyzed the dynamic response of a Class II MSMPR crystallizer. Both number concentration of crystals (zeroth moment) and total crystal surface area in suspension (second moment) were used as the controlled variables. The results presented indicate that an inherently unstable system could be stabilized by manipulation of the zeroth, but not the second, CSD moment. Of course, such a study is purely academic as there is no practical way to measure or to manipulate the CSD moments.

Stability and control for a Class I MSMPR crystallizer equipped with a fines trap was discussed by Lei, Shinnar, and Katz (1971b). In their investigation, fines crystal area was the controlled variable and either production rate or fines removal rate was the manipulated variable. They concluded that manipulation of the production rate was superior to changing the fines removal rate. Instability could be controlled only by manipulating production rate.

Beckman and Randolph (1977) developed computer simulator CYCLER to simulate the control of a Class II crystallizer equipped with fines destruction, clear liquor advance, and product classification. Two control methods were investigated. One method assumed proportional control of nuclei density using fines destruction rate as the manipulated variable. The other method used slurry density as the controlled variable and manipulated slurry withdrawal rate. Control of instability was achieved with fines manipulation but not with slurry density control, a conclusion just opposite to that of Lei et al. (1971b).

Chang and Epstein (1979) studied control strategies for Class I MSMPR crystallizers based on modal control. The basic technique used in designing a modal control was investigated by Rosonbrock (1962) and by Ellis and White (1965). The fundamental concepts of modal control are the following:

1. The dynamic behavior of a system can be depicted by the motion of a point in an  $n$ -dimensional space.
2. The  $n$ -dimensional space decomposes the system into  $n$  modes with each mode associated with one eigen-value.

3. Because the transient behavior of a process is predominantly determined by the mode corresponding to the smallest eigenvalue, the idea of this control approach is to move the eigen-values independently to a more stable or rapidly responding region.

In their analysis, residence time, seeding/fines dissolving rate, and input concentrations were considered as the manipulated variables. It was found that their control scheme could improve the performance of the linearized system for both inherently stable and unstable cases, but was not applicable for the nonlinear unstable case using the same gains as used for the linearized system.

#### Particle Size Analyzer

To implement all the control algorithms suggested above, development of an on-line instrument to measure the state of the system is necessary.

#### Laser Light Scattering Techniques

Techniques of particle-size determination by light scattering have been developed for a long time. Sloan (1955) described the use of light scattering to estimate particle diameters in the range 0.2-100  $\mu\text{m}$ . He applied an instrument designed for the angular range 0.05-140°. For low-angle scattering, Wims and Myers (1972) introduced similar instrumentation.

Farmer (1972) studied a method for determining particle size and population density in a dynamic particle field utilizing a laser

interferometer. He found that when the particle diameter was comparable to the fringe spacing the particle size could be determined. Also, when the fringe spacing was much greater than the average particle diameter, population density could be measured.

Wertheimer and Wilcock (1976) discussed light scattering measurements of particle distributions by application of a specially designed Fraunhofer plane mask. The approach was based on the concept of collecting diffracted flux in proportion to the second, third, and fourth powers of the radius of spherical particles. For any particle distribution, various statistical parameters of the distribution such as total surface area, area mean radius, and total volume could be determined. For instance, the total volume of the particles could be measured utilizing the third power mask to generate a signal proportional to the sum of the cubes of the particle radii. However, the technique could not give a complete size-frequency histogram for a distribution of sizes.

Several investigators have applied light scattering methods to applications other than crystallization. Gravatt (1973) used this technique to monitor the size distribution of particulates in air. Weiss and Frock (1976) made continuous measurements of particle distributions for a grinding process based on this method.

Felton and Brown (1979) have reported one such light scattering device for crystallization applications. They made measurements of potassium iodide crystal growth rates by laser diffraction. Seed crystals were added to a saturated solution at about 30°C in a stirred

cell and the cell was cooled slowly to room temperature. They assumed that the size distribution of potassium iodide crystals followed the Rosin-Rammler Distribution:

$$R' = \exp [-(x/\bar{x})^k] \quad [2]$$

The growth rates could be calculated from the increase of the Rosin-Rammler mean diameter ( $\bar{x}$ ) with time. However, this device is not appropriate for a continuous process.

#### Zone-Sensing Techniques

The Coulter Counter<sup>R</sup> and the Particle Data, Inc., Counter<sup>R</sup> are the two major particle-size analyzers based on the electrolyte zone-sensing principle. Particles suspended in an electrolytic solution are drawn through a small orifice with simultaneous flow of electrical current between electrodes on each side of the orifice. As each particle passes through the aperture, an electrical pulse is generated which is proportional to particle volume. The pulses are then counted and sorted to give the particle-size distribution. The method is applicable to sizes ranging from about one to two hundred microns.

Many investigators have made particle-size determinations using zone-sensing instruments. Brown (1962) applied the Coulter Counter for particle analysis of cement. Cise (1971) measured potassium sulfate crystal populations utilizing a Model T Coulter Counter and processed the data to obtain  $B^\circ$  and G values. This technique, known as the Mini-Nucleator crystallization kinetics apparatus, has been further developed and extended to other systems, e.g., Sikdar (1975, citric acid and

magnesium sulfate), Shadman and Randolph (1978, ammonium chloride), and Puri (In prep., borax). The technique has evolved to a level of sophistication wherein particles are measured with an in-line flow cell and the desired crystallization parameters  $\beta^\circ$  and  $G$  are obtained by on-line regression of the particle data using an associated minicomputer.

Rovang (1978) developed an on-line analysis method to measure growth rate and nucleation rate in a continuous crystallizer by integrating a Model T Coulter Counter into the fines loop of the crystallizer and developing on-line minicomputer processing of the population data. Rovang's work is closest to the approach taken in the present work and, in fact, both studies utilized the same bench-scale KCl crystallizer.

## CHAPTER 3

### CRYSTALLIZER THEORY

#### Process Models

Models utilizing the population balance to analyze the performance of continuous crystallizers have been proposed and examined by Randolph and Larson (1962). For a mixed-suspension crystallizer, the basic population balance is:

$$\frac{\partial n}{\partial t} + \frac{\partial (Gn)}{\partial L} + n \frac{d(\ln V)}{dt} = \sum_i \frac{n_i \vec{Q}_i}{V} + B(L) - D(L) \quad [3]$$

where  $n$  = population density at size  $L$ ;

$V$  = suspension volume;

$Q_i$  = inlet or outlet volumetric flow rate;

$B(L)$  = particle birth function at size  $L$ ; and

$D(L)$  = particle death function at size  $L$ .

This equation is averaged in external phase space and distributed in internal phase space.

For a continuous, constant-volume, isothermal MSMPR crystallizer, the complexity of equation [3] can be simplified with the following assumptions: a) steady-state operation; b) McCabe's  $\Delta L$  law, i.e., growth rate is independent of crystal size; c) clear liquor feed;

and d) negligible breakage or attrition of crystals in the stirred medium. Thus, the resultant population balance becomes:

$$\frac{Gdn}{dL} = -\frac{n}{\tau} \quad [4]$$

where  $\tau$  = residence time. Equation [4] can be integrated to give the well-known exponential population distribution:

$$n = \frac{B^\circ}{G} \exp(-L/G\tau) \quad [1]$$

where  $B^\circ/G$  is referred to as the nuclei population density. Taking the logarithm of equation [1] gives:

$$\ln n = \ln n^\circ - \frac{L}{G\tau} \quad [5]$$

Randolph et al. (1977) and Rovang (1978) have demonstrated that at steady state the particle-size distribution in the fines stream also follows the exponential form indicated by equation [1]. This is true even when the product crystals are undergoing transient changes. Thus, using the linear regression of  $\ln n$  against  $L$ , the slope can be used to determine the growth rate and the intercept provides the value of nucleation rate. Particle statistics of interest obtained from regression of the exponential distribution are listed below:

1. Number mean size:

$$\bar{L}_{10} = \frac{\int_0^{\infty} LndL}{\int_0^{\infty} ndL} \quad [6]$$

2. Weight mean size:

$$\bar{L}_{43} = \frac{\int_0^{\infty} (\rho k_v L^3) L n dL}{\int_0^{\infty} \rho k_v L^3 n dL} = 4G\tau \quad [7]$$

3. Total number:

$$N_T = \int_0^{\infty} n dL = B^{\circ} \tau \quad [8]$$

#### Interrelationship between $B^{\circ}$ , $G$ , $s$ , and CSD

The two steps of nucleation and crystal growth occur in parallel in the process of crystallization. Theoretical considerations predict that both nucleation and crystal growth are functions of supersaturation and interact strongly with CSD as illustrated in Figure 1 (Randolph and Larson, 1971). The degree of supersaturation is determined by the production rate and the total crystal surface area available for deposition. Supersaturation then determines growth and nucleation rates. The crystal size distribution is, in turn, determined by the interaction between growth and nucleation rates with the particle residence-time distribution (expressed as a function of flow versus size in the population balance). Since the crystal surface area is a function of the size distribution, the interrelationship forms a feedback loop.

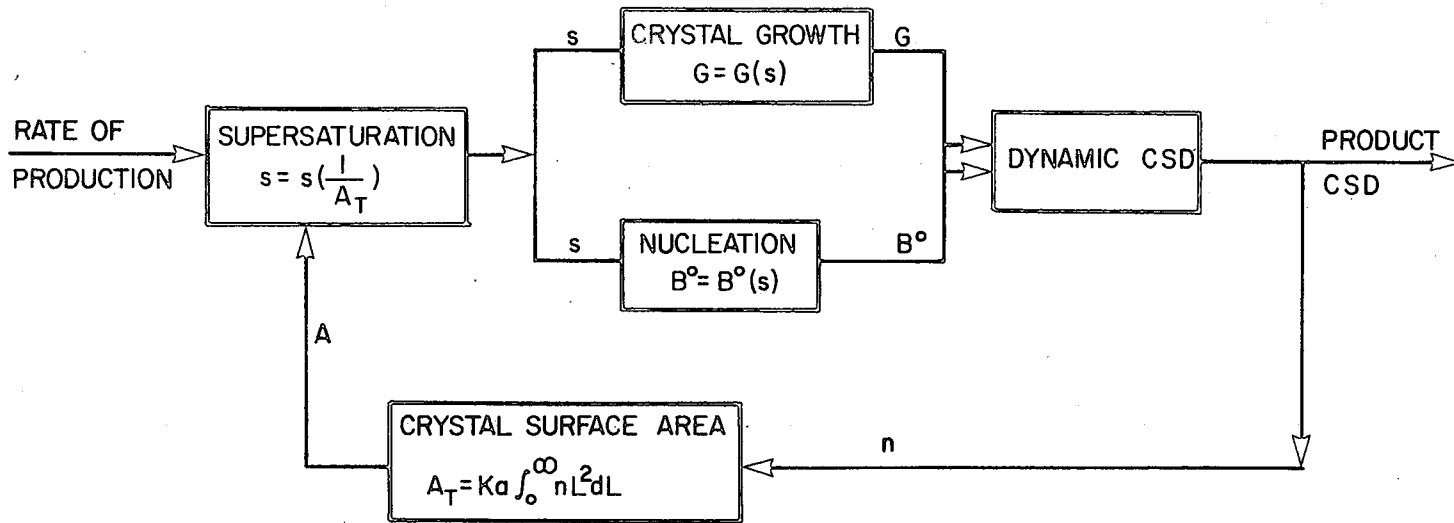


Figure 1. Interrelationship between Nucleation Rate, Growth Rate, Supersaturation, and Crystal-Size Distribution.

### Nucleation Kinetics

In crystallization processes, the formation of nuclei in a supersaturated solution can occur in three different ways: homogeneous nucleation, heterogeneous nucleation, and secondary nucleation. Homogeneous nucleation is the formation of new crystals as a result of supersaturation only. Heterogeneous nucleation is the appearance of nuclei due to the presence of foreign particles (substrates). Secondary nucleation is induced by the presence of seed crystals of the material being crystallized. Much recent research has been centered around secondary nucleation as this mechanism is dominant in most industrial crystallizers.

Secondary nucleation rate can often be correlated with the simple power-law model:

$$B^{\circ} = k_n (\text{temperature, RPM}) G^i M_T^j \quad [9]$$

In equation [9], the slurry density,  $M_T$ , represents the concentration of crystals in the magma. The growth rate,  $G$ , is assumed to be a linear function of supersaturation. The rate constant,  $k_n$ , accounts for the effect of temperature and agitation rate on nucleation. A model of this form has been used successfully to correlate nucleation rate data by many investigators (e.g., Randolph and Cise, 1972; Randolph and Youngquist, 1972; Juzaszek and Larson, 1977; Puri, In prep.).

### Control Algorithm

In Chapter 2, several algorithms for the control of particle-size distribution in crystallizers were discussed. This section will discuss in more detail the control method proposed by Beckman and Randolph (1977).

Utilizing the computer simulator CYCLER, Beckman and Randolph (1977) developed a successful control method which might be applicable to industrial complex crystallizers using nuclei density as the controlled variable and fines destruction as the manipulated variable. The following proportional-control algorithm was used:

$$\left( \frac{R}{\bar{R}} - 1 \right) = K_c \left( \frac{n^\circ}{\bar{n}^\circ} - 1 \right) \quad [10]$$

The value of  $K_c$ , which guarantees control, was determined as:

$$K_c \geq \frac{\left( 1 - \frac{R_s}{\bar{R}} \right)}{(i-1)} \quad [11]$$

where  $R$  = normalized fines destruction rate (compared to MSMPR flow);

$K_c$  = proportional control constant;

$n^\circ$  = nuclei density.

$R_s$  = critically stable fines destruction rate; and

$i$  = relative nucleation/growth sensitivity exponent in kinetics model.

The superscript "<sup>-</sup>" indicates a steady-state value which is the target value sought by control. It was found that a  $K_c$  value of 0.25 would completely eliminate the limit cycle behavior of classified crystallizers.

Beckman and Randolph's (1977) study assumed perfect knowledge of population densities in the fines loop, i.e., from computation using Program CYCLER. The nuclei density was determined by a least-squares extrapolation to zero size using calculated population densities at small particle sizes. To accomplish this control algorithm experimentally would require the development of new on-line particle measurement technologies. The present study is motivated by the CSD control study of Beckman and Randolph (1977).

## CHAPTER 4

### EXPERIMENTAL

Descriptions of the main elements of the apparatus as well as the experimental procedure are presented in this chapter.

#### Description of Equipment

The system used for the measurement of crystallization rate is shown schematically in Figure 2 and is similar to the one reported by Rovang (1978). The major components of this experimental set-up are as follows:

1. Feed tank.
2. Crystallizer and fines trap.
3. Crystallizer cooling system.
4. Fines destruction system.
5. Sampling system.
6. Particle-sizer and analysis system.

#### Feed Tank

The feed tank, with a capacity of 200 liters, was made from Epoxy fiberglass and was divided into two equal-volume compartments by a doughnut-shaped baffle. The lower compartment received the mixed product discharge and overflow from the crystallizer to form a "closed system" and always maintained excess crystal solids to assure

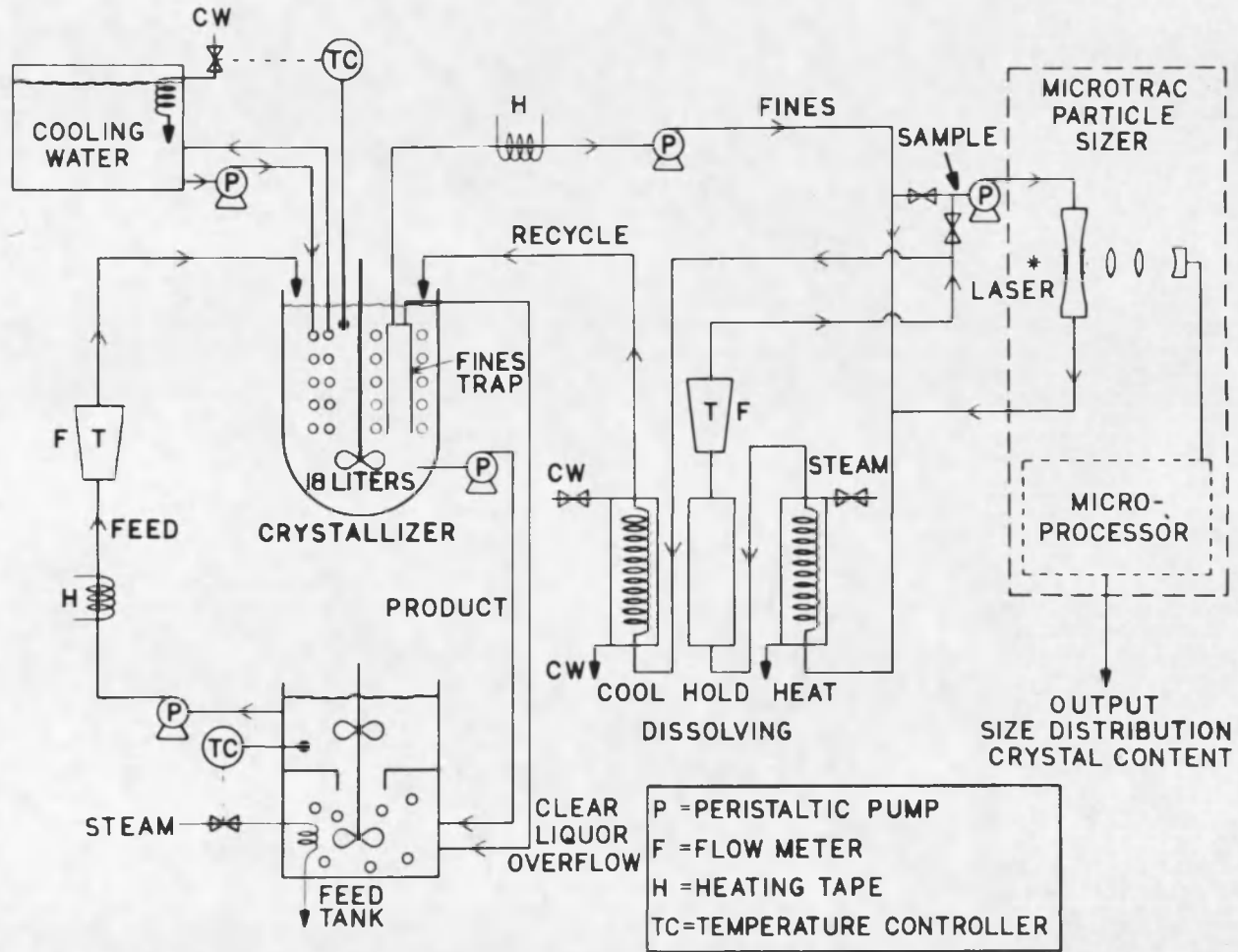


Figure 2. Schematic Diagram of Experimental Equipment.

saturation. Saturated solution moved from the lower compartment to the upper compartment where it was fed to the crystallizer. Brine saturated with KCl (and partly saturated with NaCl and  $MgSO_4$ ) was well-agitated by stainless steel marine impellers attached to a central shaft driven by a 1/15 HP variable speed Dayton gearmotor.

The feed temperatures used varied from 145° to 165°F, corresponding to crystal production rates of approximately 50 to 80 g/liter of feed solution. The constant temperature in the feed tank was achieved by using a modified Dayton thermostat which regulated the flow of 40 psig steam through the heating coils in the lower compartment. In order to assure that the feed stream was particle free, the feed was heated by a six-foot length of 3/8" stainless steel tubing wrapped with heating tape. The temperature in this line was controlled by a rheostat.

#### Crystallizer and Fines Trap

The crystallizer was an Epoxy fiberglass tank of 18 liters working volume. Inside the crystallizer, there were two sets of fixed concentric 1/2" and 3/8" stainless steel coils having 4" and 8" diameters, respectively. The outer coil was held in the crystallizer by three vertical baffles and was wound around a draft tube. The inner coil was also held by three vertical baffles connected to the draft tube. The slurry in the crystallizer was well-mixed by a stainless steel marine impeller which forced the suspension to flow down the center of the crystallizer and up the outside of the annulus. A crystallizer temperature of 100°F was used and was controlled by tempered cooling water flowing through the coils.

An internal fines trap (gravity settling in an inverted chamber) was located in the annular area between the outer and inner cooling coils in the crystallizer. The trap was made of Plexiglass and could classify crystals with a cut-size around 150 to 200  $\mu\text{m}$ . Two streams came out of the fines trap; namely, clear liquor overflow (for level control and manipulation of solids content) and the fines stream. A schematic drawing of the fines trap is shown in Figure 3.

#### Crystallizer Cooling System

The three major components of the cooling system are: two centrifugal pumps in series, a blend tank, and the crystallizer cooling coils. Fresh cooling water was blended with the warm circulating water in the blend tank. With this arrangement, fouling on the coils was minimized by operating with the lowest temperature difference necessary to maintain the crystallizer temperature.

#### Fines Destruction System

The fines destruction system consisted of a steam heater, a hold tank, a water cooler, and a peristaltic pump. The fines stream was removed from the fines trap by the peristaltic pump. Fines destruction was achieved by raising the fines stream temperature by 30-40°F, holding for a short while, then cooling and returning to the crystallizer.

#### Sampling System

The fines stream was withdrawn continuously from the fines trap by a peristaltic pump. Before passing through the fines destruction heater, a sample flow from the fines stream went to the on-line particle

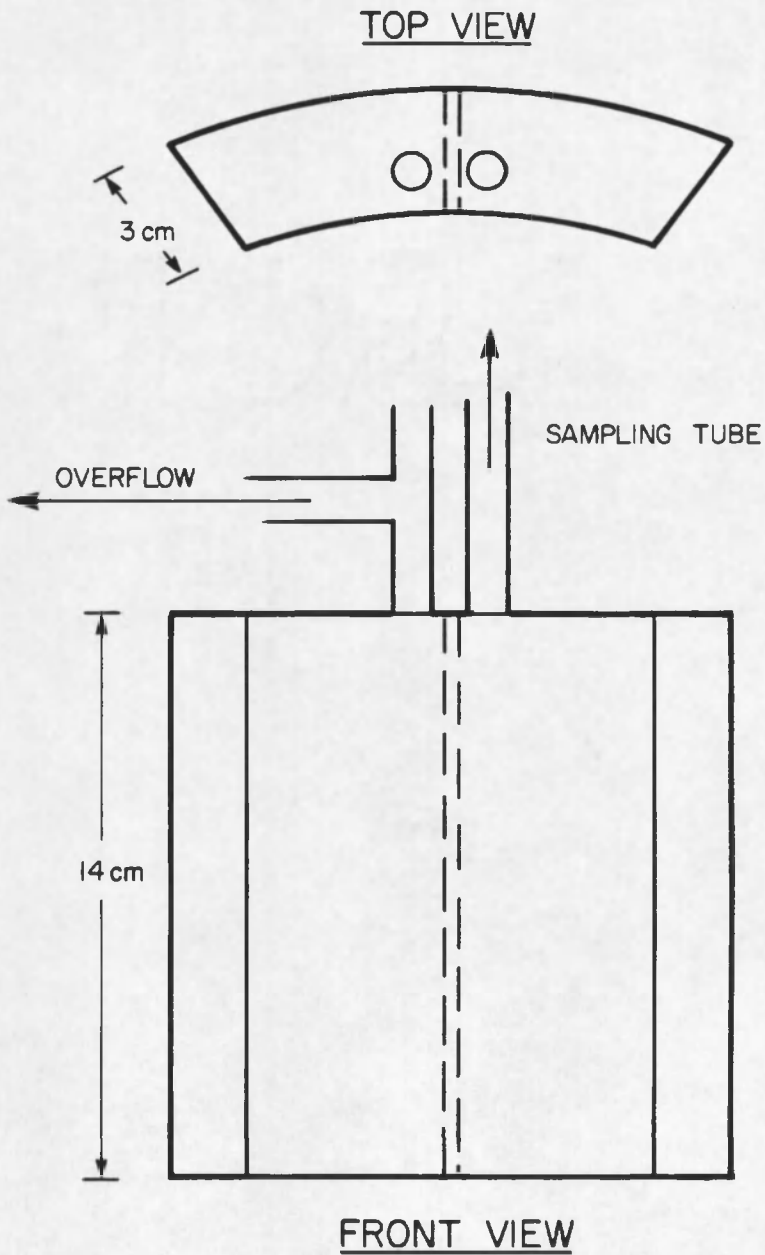


Figure 3. Schematic Drawing of Fines Trap Device.

analyzer and then returned to the fines stream. Another flow which was used periodically for background correction also went to the on-line sizer after fines destruction. The sample line flow diagram is shown in Figure 4.

#### Particle-Sizer and Analysis System

A low-angle, forward light scattering particle-size analyzer was used to measure the particle-size distribution of the fines stream. As shown in Figure 5, the particles suspended in the sample flow pass through the sample cell where they pass through a laser beam. Each particle will scatter light in a forward direction with an intensity and angle which depends on its size. The intensity of the scattered light at various angles is collected by a lens, passed through an optical filter, and focused by a second lens onto a photocell detector. With particles of different sizes present in the laser beam, the relative intensities at various angles can be manipulated to give the size distribution. These calculations are performed digitally within the instrument's microprocessor.

Because only the relative intensities at the various scatter angles are necessary to determine the size distribution, the results are independent of sample time, velocity through the cell, and particle concentration. The statistical accuracy of the results are better, of course, if reasonable sample times (1 to 5 minutes) are used. Moreover, if the particle concentration becomes too high, say greater than 0.1% by volume, multiple scattering of the light occurs and performance of the

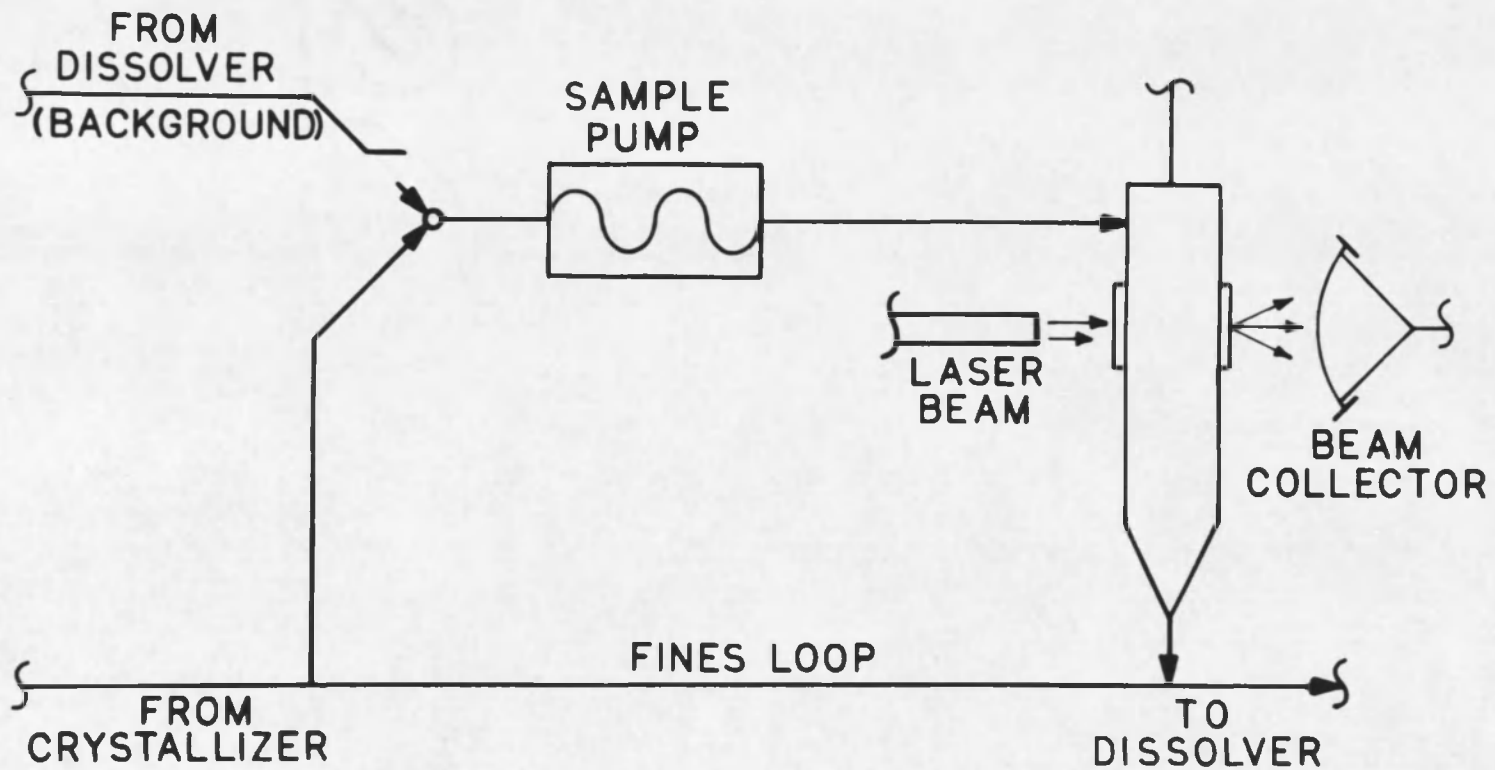


Figure 4. Sample Line Flow Diagram.

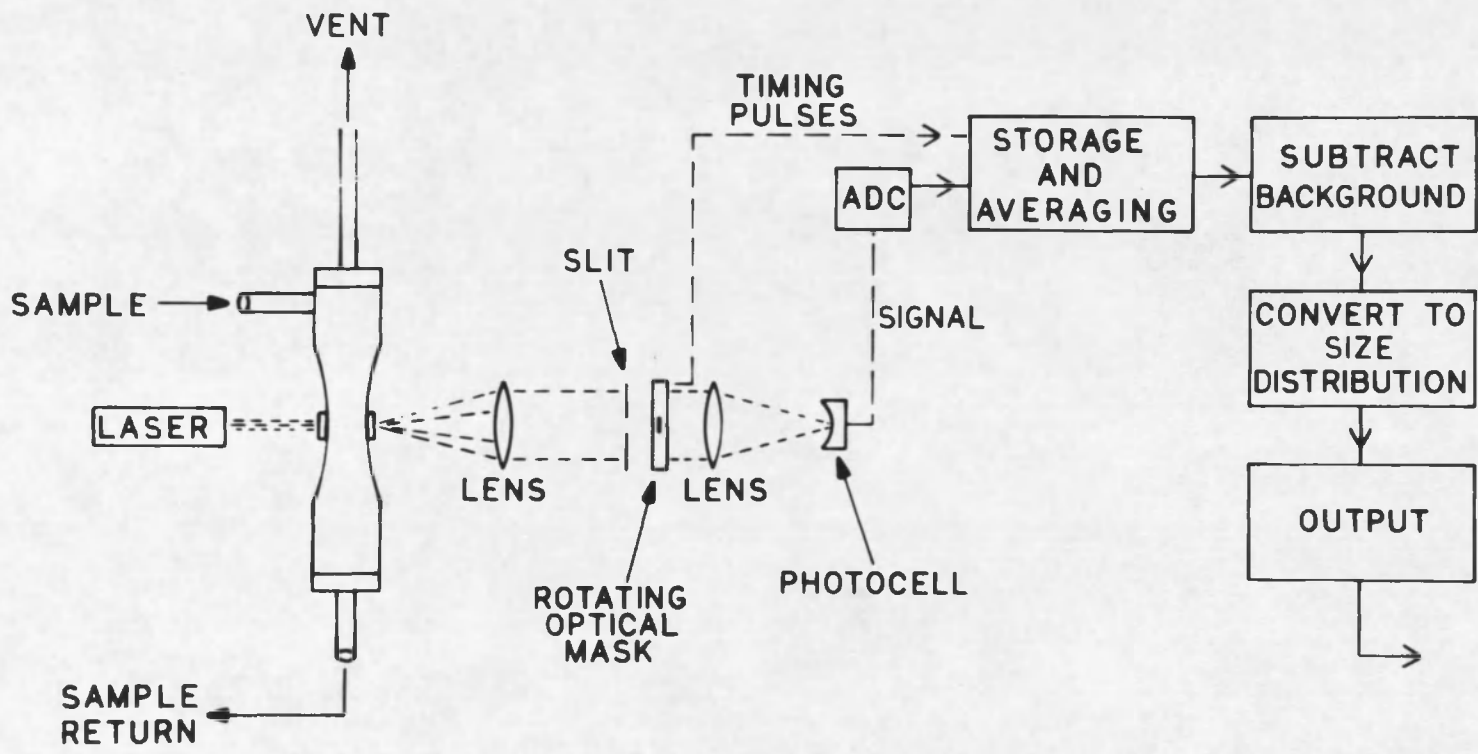


Figure 5. Light Scattering Particle-Size Analyzer.

instrument deteriorates. Nevertheless, the instrument is capable of operating over a wide range of sample conditions.

The particle-size analyzer provides a 13-channel histogram of size distribution over the range of 1.9 to 176  $\mu\text{m}$  in a square-root-of-two series, as well as some common statistical measures of size distribution, e.g., mean diameter of the volume distribution and mean specific surface area. Also available was the particle concentration (crystal content) which was determined from the total intensity of the scattered light.

Because the particle sizer only senses the volume of particles in each size range, a necessary requirement is to convert the volume distribution to the population distribution. This job was done by coupling the particle sizer to the SPC-16, real-time minicomputer front-ended with a KIM-1 microprocessor and a LA-36 Decwriter, using the following equation:

$$n(L) = \frac{M_{Tf} \Delta W}{\rho k_v \bar{L}^3 \Delta L} \quad [12]$$

where  $M_{Tf}$  is the solids concentration in the fines loop and  $\Delta W$  is the volume fraction of crystals in the size range  $L$  to  $L+\Delta L$ . The value of  $k_v$  is equal to  $\pi/6$  as the instrument was calibrated with spheres. Once these population densities were calculated, a linear regression of data was performed by the minicomputer to give growth rate, nuclei density, and nucleation rate. Also available was a statistical analysis which could show the reliability of the determined parameters. An information

flow diagram is given in Figure 6. A typical computer printout of the data reduction results is presented in Appendix A.

### Experimental Procedure

In this section, a description of the instrument tests, operation of equipment, and start-up and shut-down procedures are included.

#### Instrument Tests

The particle-size analyzer was tested against some known particle-size distributions before application to the crystallizer. Both de-aerated isobutanol and saturated KCl solutions were circulated through the cell and known concentrations of KCl crystals or other calibrating particles were added. Initial de-aeration was necessary because the particle sizer also measures bubbles as particles. KCl crystals were mixed from sieved fractions so as to have size distributions similar to those expected in the fines loop. Also, several other narrow-sieved fractions were tested, such as glass beads and garnet samples, which were supplied by the manufacturer. Both a Model ZBI Coulter Counter<sup>R</sup> and a Particle Data, Inc., Counter<sup>R</sup> were used for size comparisons of the calibration samples. The results from these calibration tests and analysis of the instrument errors are discussed in Appendix B.

It was found that the output from the particle sizer could not be considered sufficiently reliable for this study unless the channel contained at least 5% of the volume of crystals. Since the size distribution of the fines followed the exponential distribution, this meant

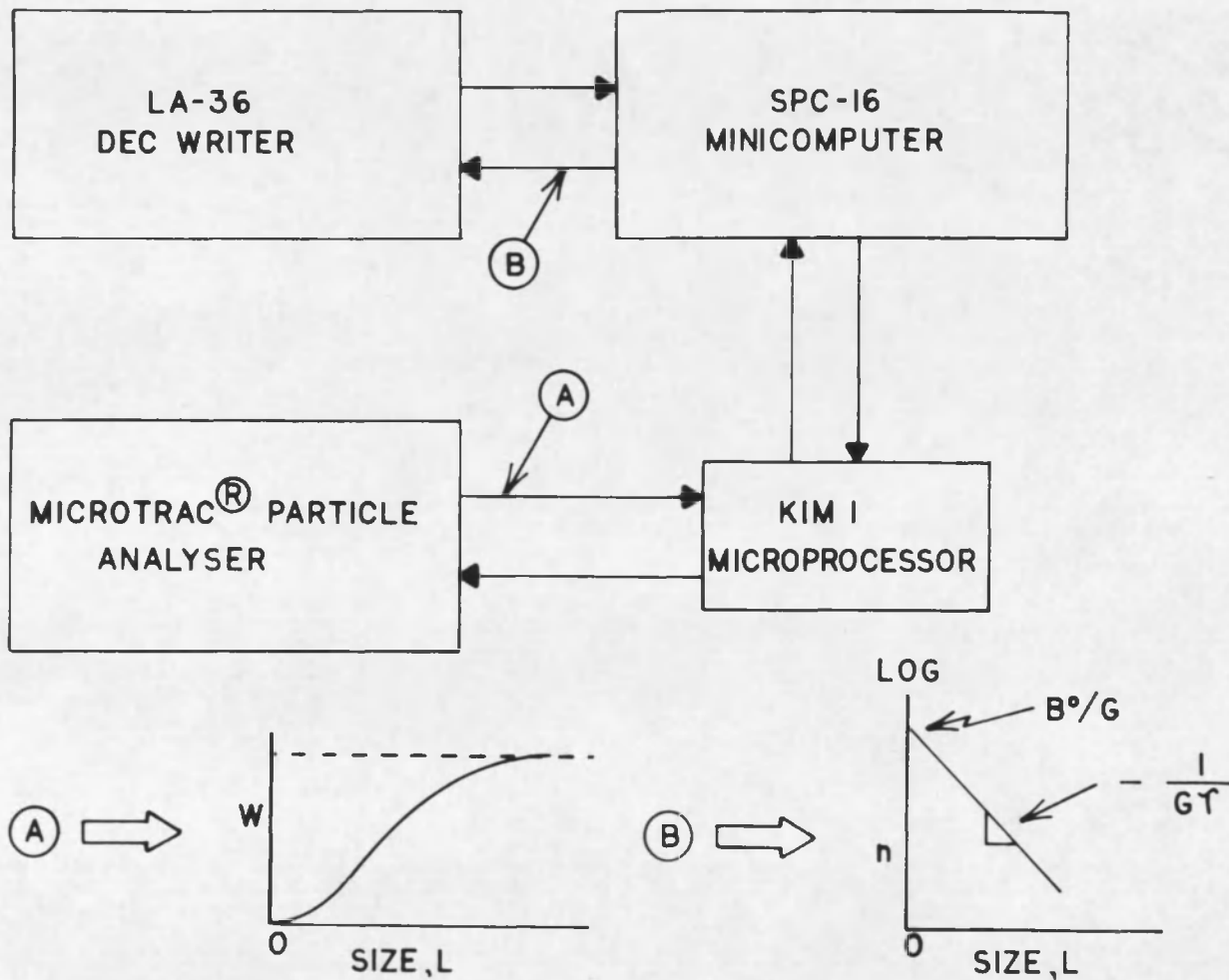


Figure 6. Information Flow Diagram.

that no more than 6 of the size channels could be used. These were centered about the mass mean size  $\bar{L}_{43}$ . This represents a different size range, encompassing larger sizes, than those covered by zone-sensing instruments.

#### Operation of Equipment

Initial experimental runs were made to shake down the crystallization apparatus and identify the operating ranges. Many operating problems were encountered, as follows:

1. Persistent plugging of the flow lines.
2. Air bubbles sucked into the fines loop through unsealed fittings.
3. Crystallization on the cell windows or the walls due to the supersaturated solution.
4. The on-line minicomputer system would "crash."
5. Fouling of the sample line due to too slow sample flow.
6. Over-dissolving nuclei due to turning on the fines destruction system before a seed bed was established.
7. Feed flow rates were either above or below the operable range.
8. Mechanical problems of the equipment, e.g., worn tubing in the peristaltic pump, agitator shaft corrosion, etc.

All of these problems were solved by making some modifications in the equipment and/or by improving experimental methods. After these problems were solved in shakedown runs, the equipment ran consistently for the remainder of the experimental program.

## Start-Up

Each experiment was begun by filling the crystallizer with cold mother liquor from a previous run. This minimized initial fouling of the crystallizer cooling coils. Then the crystallizer agitator, the feed tank agitator, and the feed pump were started. The cold feed stream passed into the crystallizer and overflowed to the feed tank. Next, the feed tank temperature controller, the feed line heating tape, and the steam to the feed tank were turned on. At this point, the feed tank would gradually warm up and bring warmer, richer feed to the crystallizer. The crystallizer cooling system would automatically take over when the crystallizer temperature reached the set point (100°F). After the crystallizer had reached 100°F and temperature control was working, the crystallizer was seeded with recrystallized solids from the previous run. Feeding was continued until all the flows and temperatures were constant. After the crystallizer had visibly nucleated, the fines destruction system was started. Care was necessary because starting the fines destruction system too early often over-dissolved the nuclei. The crystallizer was left on total overflow until the slurry density built up to the expected operating level. At this point, the product pump was turned on. The feed rate and the fines removal rate were adjusted to the desired setting using in-line calibrated flowmeters. The product rate was set with a cycle-timer using a graduated cylinder and stopwatch. After the run had stabilized, both the Microtrac and the real-time computer analysis systems were started. The background counts for the Microtrac were set in the Microtrac memory by

circulating the dissolved fines flow back through the cell. After all of these tasks were accomplished, samples could be taken and an initial steady state observed and/or a planned disturbance made to the system.

#### Shut-Down

The first step of the shutdown procedure was to turn off all the heating tapes and steam. The Microtrac and product pump were then turned off and the feed pump was reversed to clear the feed line. The fines pump was also reversed to force the fines stream back to the crystallizer which overflowed to the feed tank. The slurry retained in the crystallizer was drained into a hold tank and saved for the next run. The crystallizer and all lines were flushed with water to remove crystal residues and the water was then drained. The crystallizer agitator and all the pumps were then turned off. However, the feed tank agitator was left running during the feed tank cool-down period to form crystals. Otherwise, a solid scale would build up in the feed tank which would damage the agitator when it was restarted.

## CHAPTER 5

### EXPERIMENTAL RUNS

#### Experimental Conditions

A series of full-day experiments was performed on the crystallizer with the Microtrac on-line in the fines loop to track specific crystallizer dynamic responses to known upsets. The output from the Microtrac was analyzed by the SPC-16 minicomputer, giving the regression constants  $B^\circ$  and  $G$  as well as various statistics. Samples were taken every few minutes. The calibration relation between the Microtrac output and solids concentration was initially fed into the minicomputer.

Under operating conditions, the mass mean size of the fines was about 100  $\mu\text{m}$  ( $G\tau \sim 25 \mu\text{m}$ ). This meant that only 4 channels contained data of sufficient accuracy for use. The largest size range (125 to 176  $\mu\text{m}$ ) contained an appreciable percentage of the size distribution; however, this value was distorted because it covered the classifier cut-size range and it was not used in the regression. Thus, each regression was based on 4 data points (channels 9 to 12) covering the size range 31 to 125  $\mu\text{m}$ .

The procedure in each test run was to bring the crystallizer to steady state, then perturb it by changing one variable at a time and follow the dynamics resulting from that change. The variables studied

and their operating ranges are given in Table 1. A summary of the operating conditions for the individual experiments is given in Table 2.

### Results

Run 5/22/79/SS-1 was performed to evaluate the time required to come to a steady-state response. Figure 7 represents the results. The solids concentration in the fines loop ( $M_{Tf}$ ), growth rate ( $G$ ), and nucleation rate ( $B^\circ$ ) were plotted on ordinary and semilog paper against time to present a clear view of the time behavior of the crystallizer during the run.

Run 6/13/79/RP-2, Run 7/31/79/RP-3, and Run 9/5/79/RP-4 were done to study the response to changes in agitation; the results are given in Figures 8, 9, and 10, respectively. The dissolver fines,  $M_{Tf}$ , and nucleation and growth rates,  $B^\circ$  and  $G$ , were observed and recorded as well as slurry density in the crystallizer to indicate the overall state of the system. The slurry density was measured every half hour by vacuum filtering the product stream with a 350-ml sintered glass buchner funnel and drying the solid crystals with saturated acetone. The slurry density was calculated as solids weight per unit volume of clear solution.

Run 5/17/79/QF-1, Run 6/26/79/QF-3, and Run 8/21/79/QF-4 were made to show the responses to a fines dissolution rate change. The fines rate was increased for the first run and decreased for the second and third runs after the system had approximately reached steady state. Figures 11, 12, and 13 show the results from these three runs. Two more

Table 1. Variables Studied and Operating Ranges.

Variable	Range
Fines rate	800-1700 cc/min
Stirrer speed	480-550 rpm
Feed rate	300-450 cc/min

Table 2. Experimental Operating Conditions.

Run	Feed (cc/min)	Fines Removal (cc/min)	Product (cc/min)	RPM
5/15/79/QI-1	300/425	1000	180	480
5/17/79/QF-1	300	1000/1700	180	480
5/22/79/SS-1	400	1000	180	480
6/13/79/RP-2	400	1000	150	550/480
6/20/79/QF-2	400	800	150	480
6/26/79/QF-3	400	1500/1000	150	480
7/31/79/RP-3	400	1000	200	480/500
8/02/79/QI-3	400/320	1000	200	480
8/21/79/QF-4	360	1400/1000	190	480
8/29/79/QI-4	320/400	1000	190	480
9/05/79/RP-4	350	1200	190	480/520

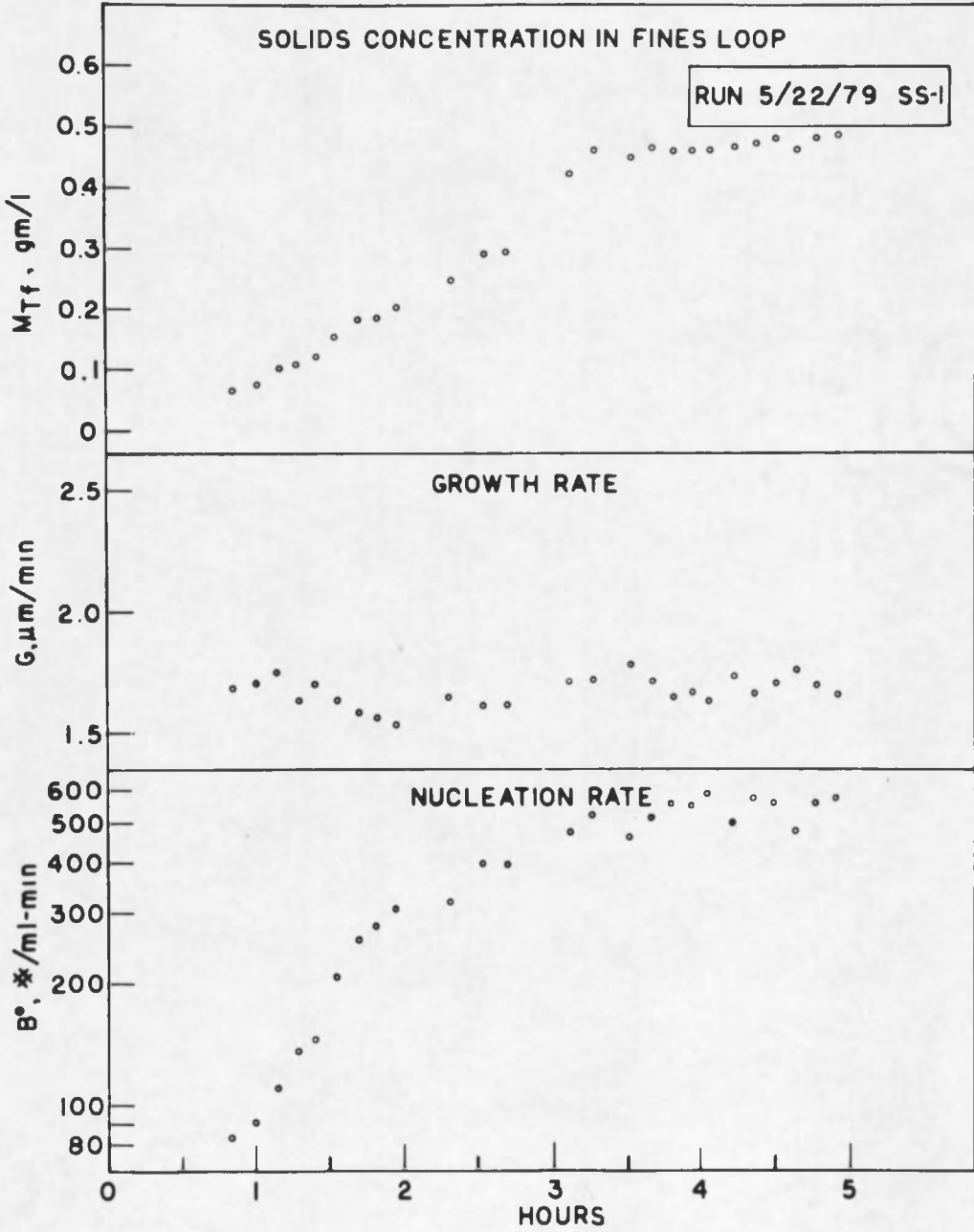


Figure 7. Response at Steady State, Run 5/22/79/SS-1.

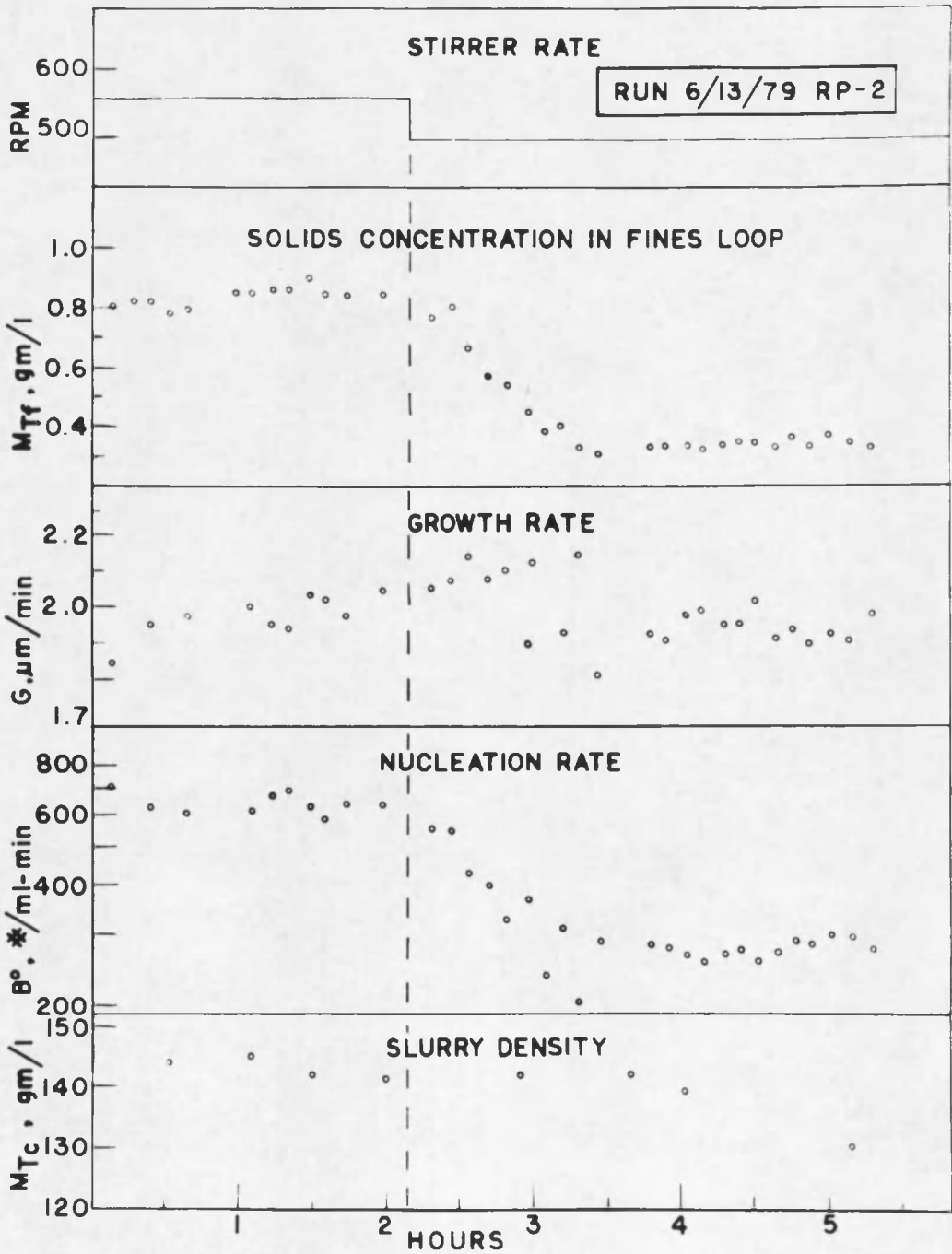


Figure 8. Response to an Agitator Speed Decrease, Run 6/13/79/RP-2.

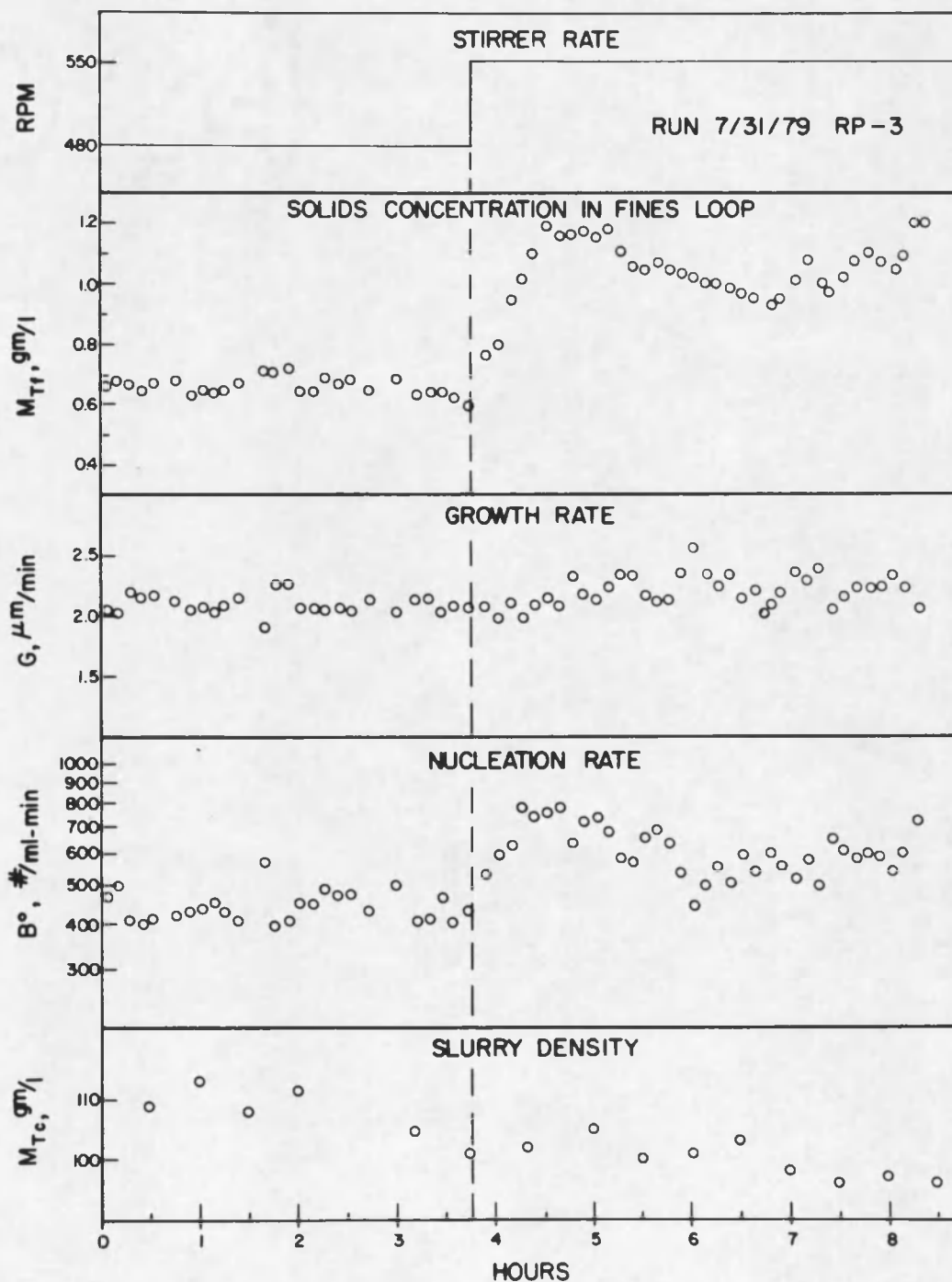


Figure 9. Response to an Agitator Speed Increase, Run 7/31/79/ RP-3.

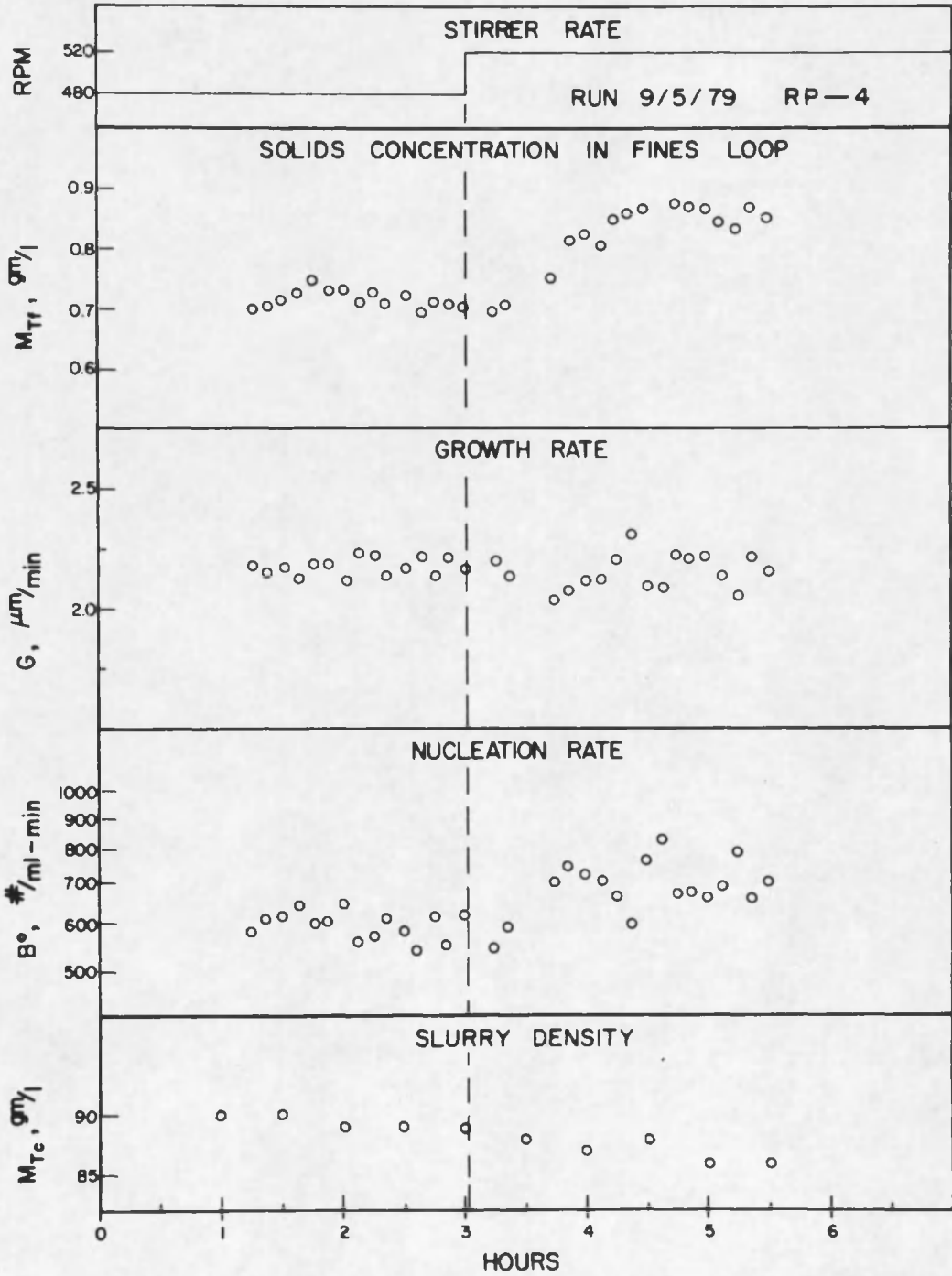


Figure 10. Response to an Agitator Speed Increase, Run 9/5/79/RP-4.

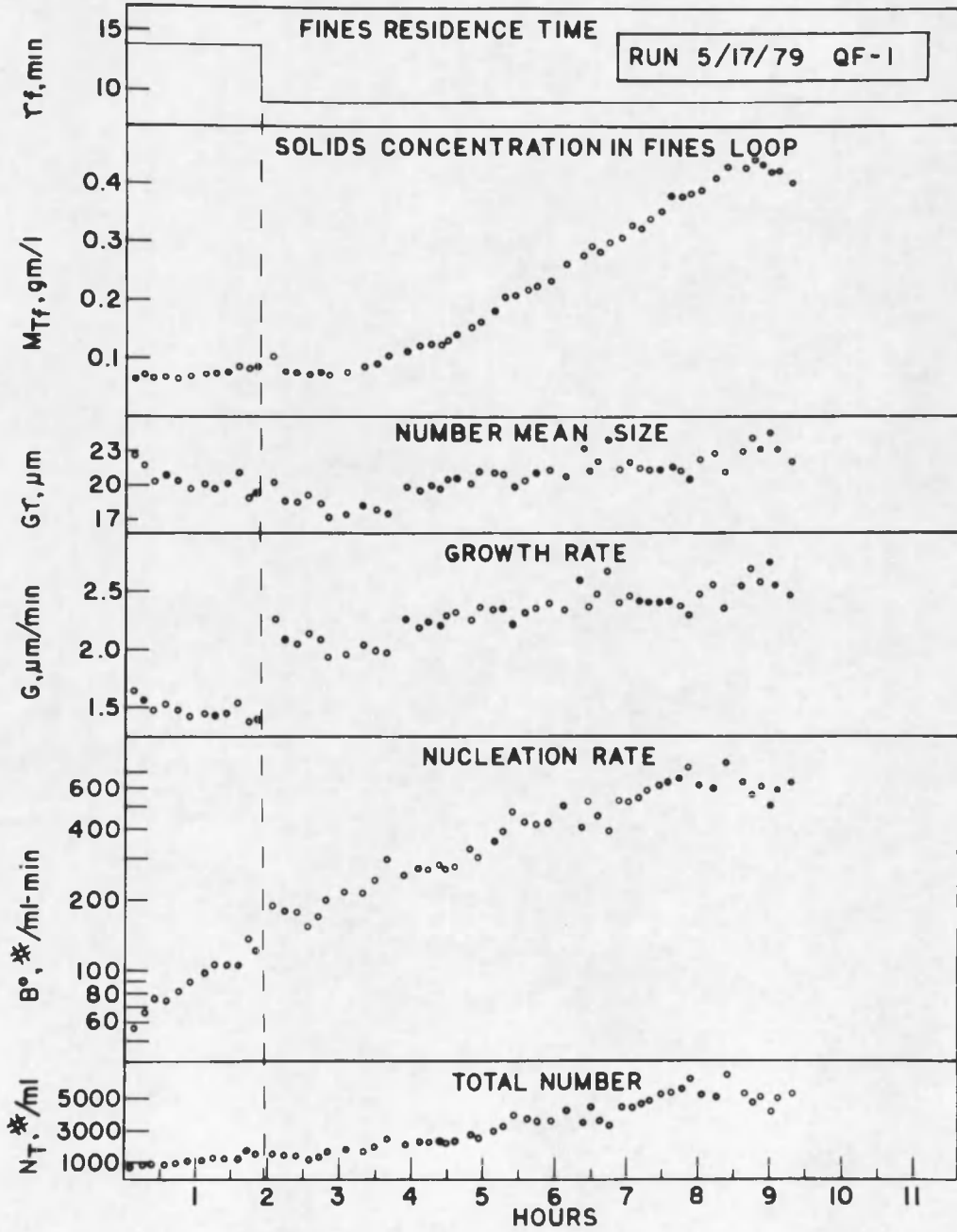


Figure 11. Response to a Fines Dissolution Rate Increase, Run 5/17/79/QF-1.

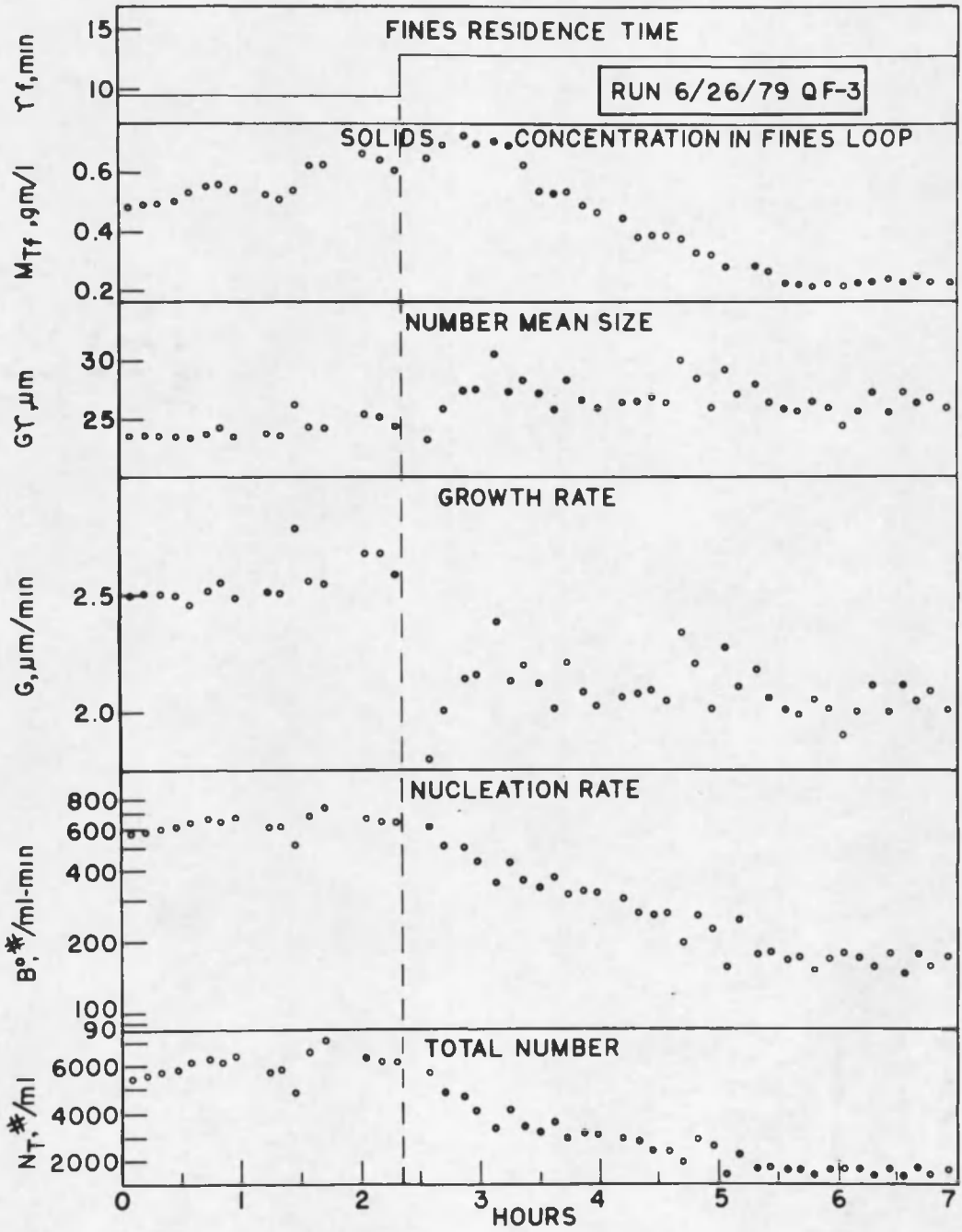


Figure 12. Response to a Fines Dissolution Rate Decrease, Run 6/26/79/QF-3.

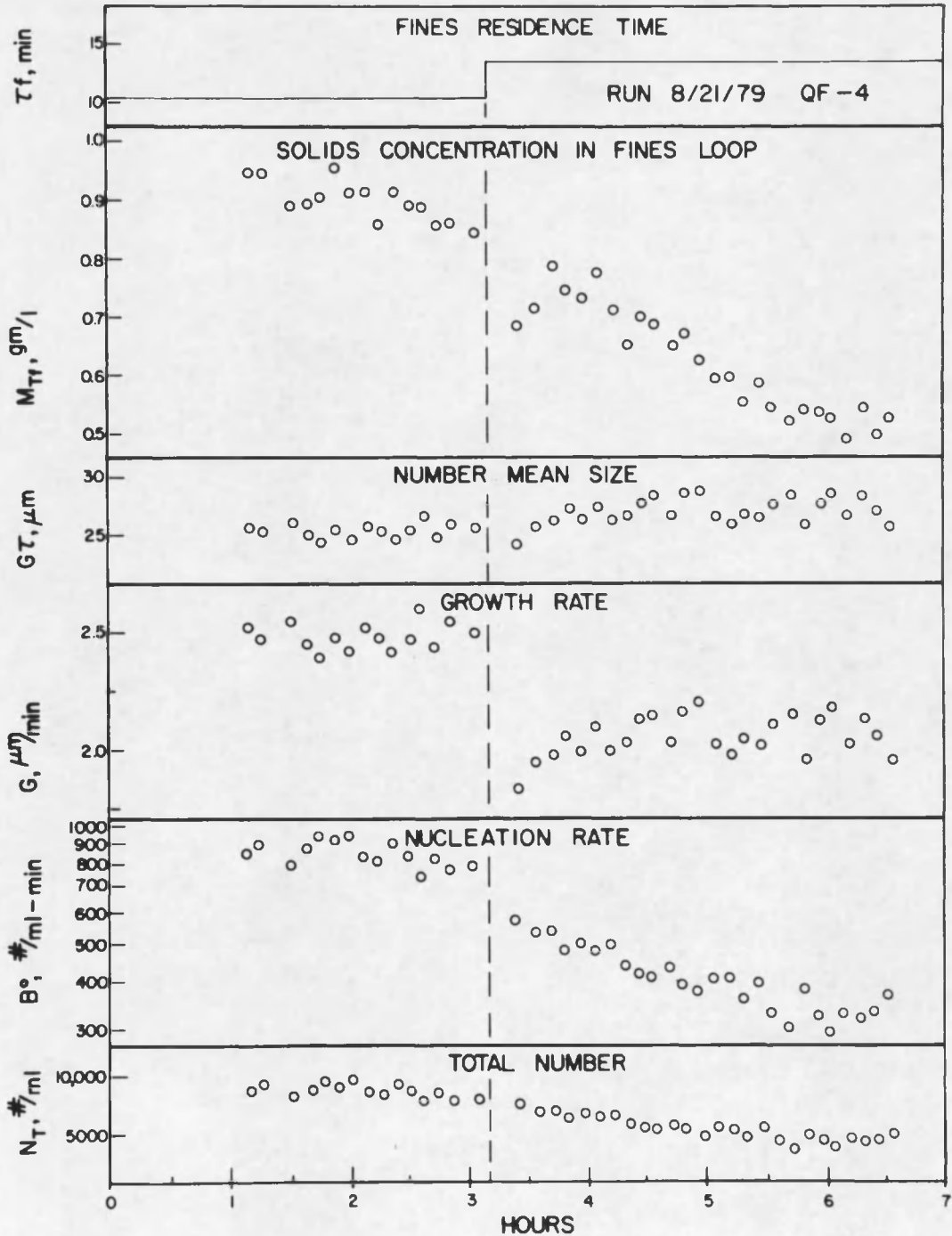


Figure 13. Response to a Fines Dissolution Rate Decrease, 8/21/79/QF-4.

state variables, the number-mean-size and total number, are included in the figures.

A step change in feed rate was introduced in Runs 5/15/79/QI-1, 8/2/79/QI-3, and 8/29/79/QI-4. Both increases or decreases in feed rate were used to test the response of the crystallizer. Figures 14, 15, and 16 show the measured responses of solids concentration, growth rate, and nucleation rate in the fines loop.

Figure 17 shows an inadvertent temperature upset response of the crystallizer for Run 6/20/79/QF-2. This upset was caused by an accidental interruption of crystallizer cooling water for about 25 minutes, after which time the coolant was restored.

These dynamic responses are discussed in more detail in the following chapter.

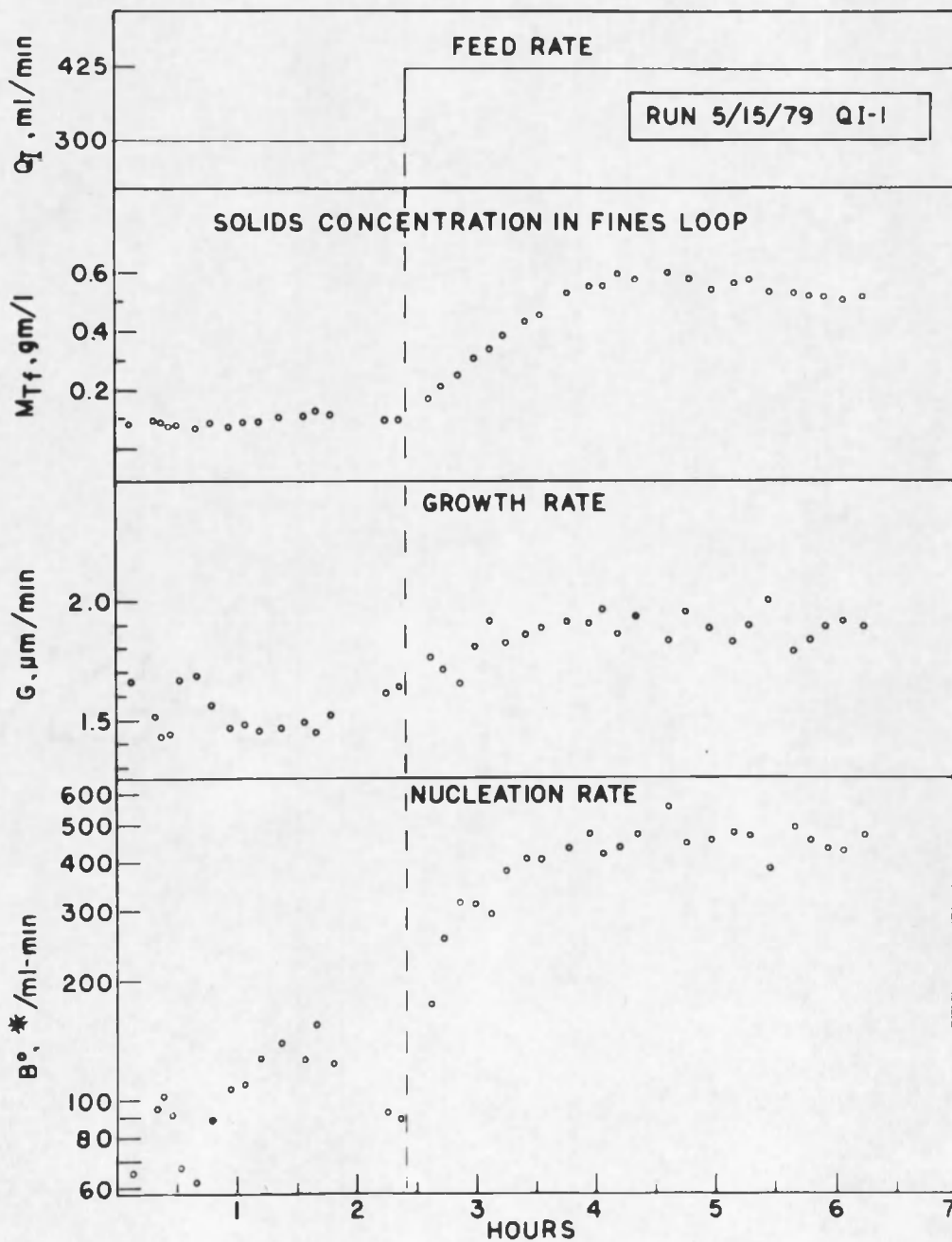


Figure 14. Response to a Feed Rate Increase, Run 5/15/79/QI-1.

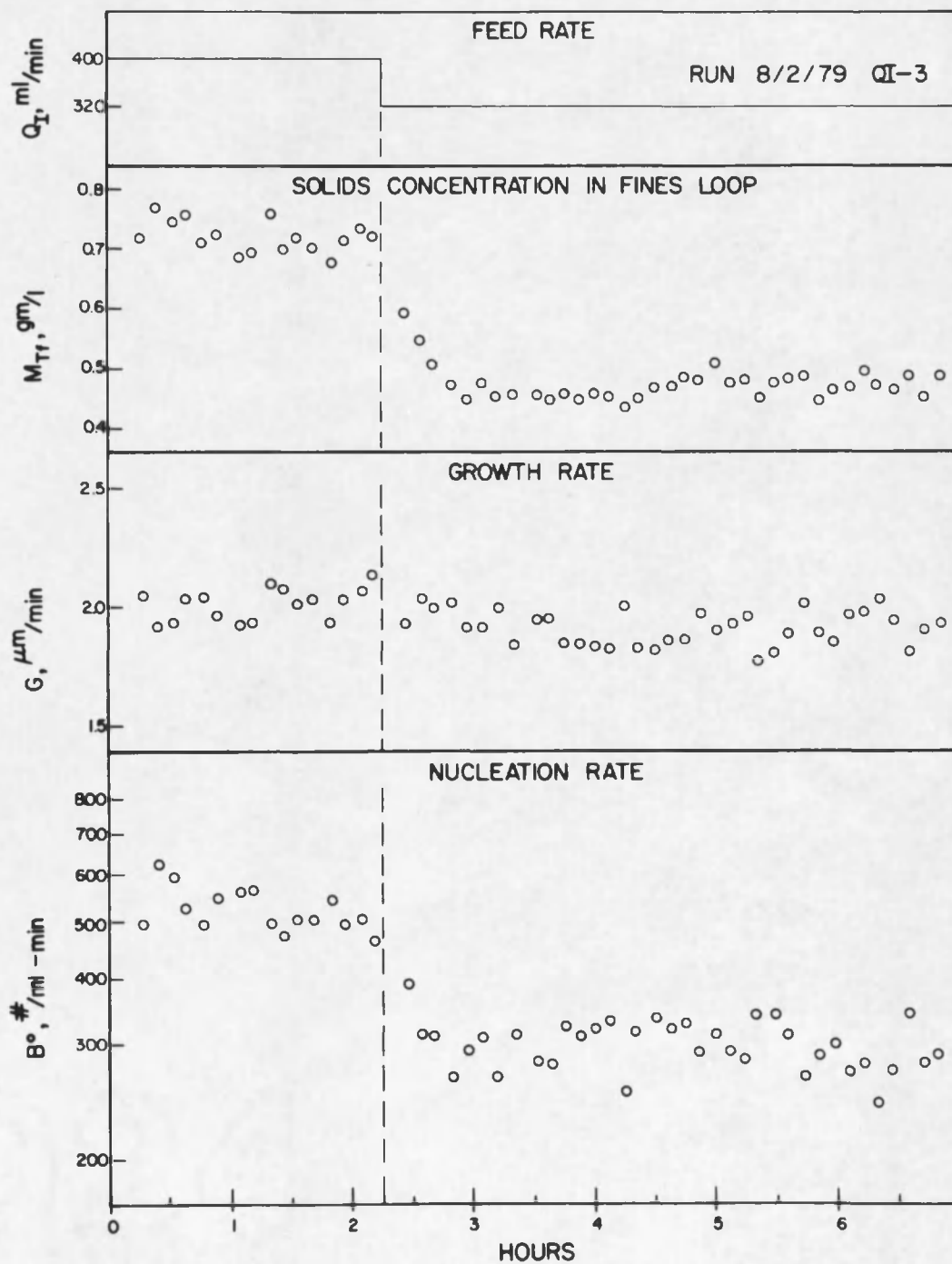


Figure 15. Response to a Feed Rate Decrease, Run 8/2/79/QI-3.

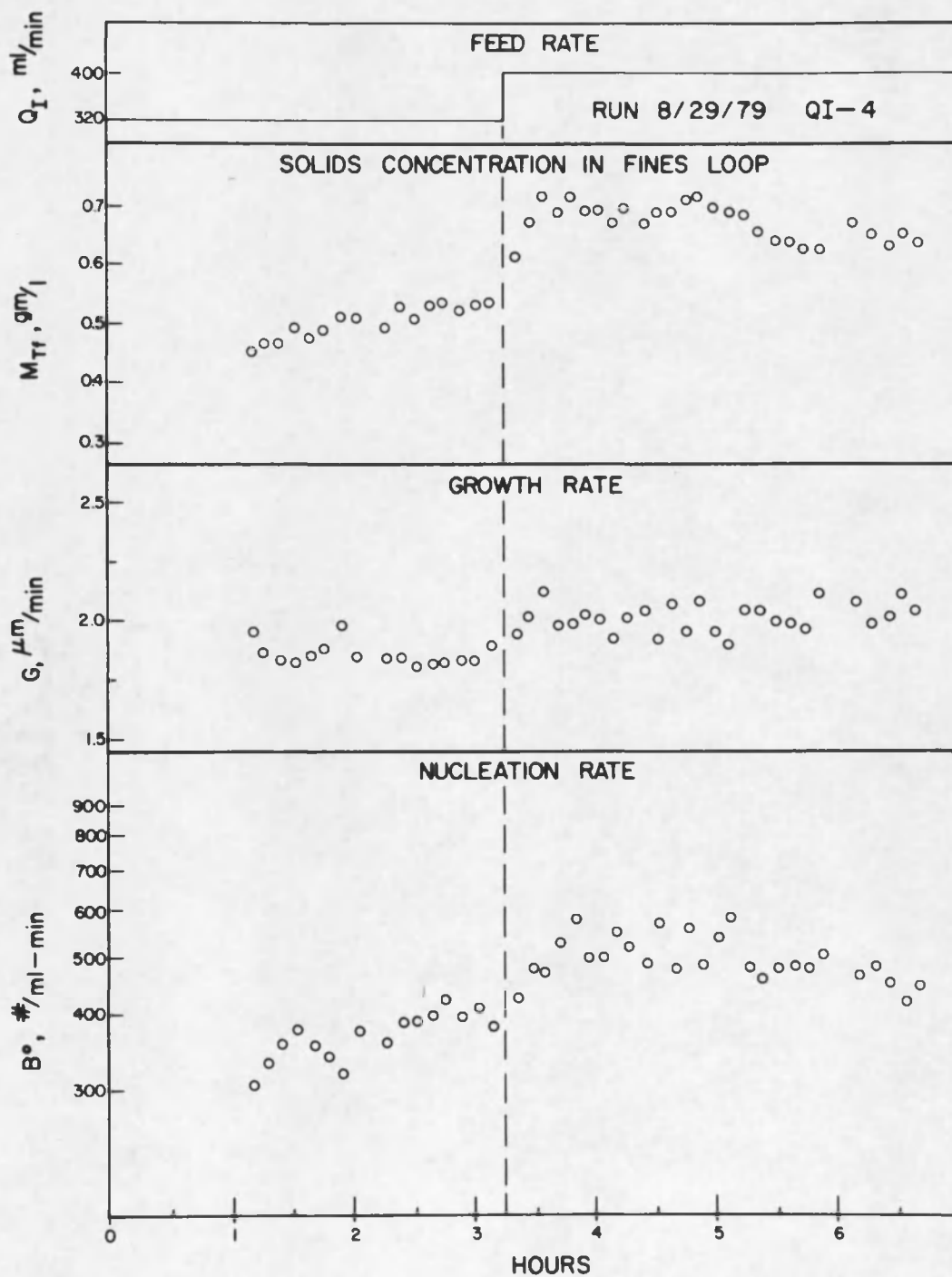


Figure 16. Response to a Feed Rate Increase, Run 8/29/79/QI-4.

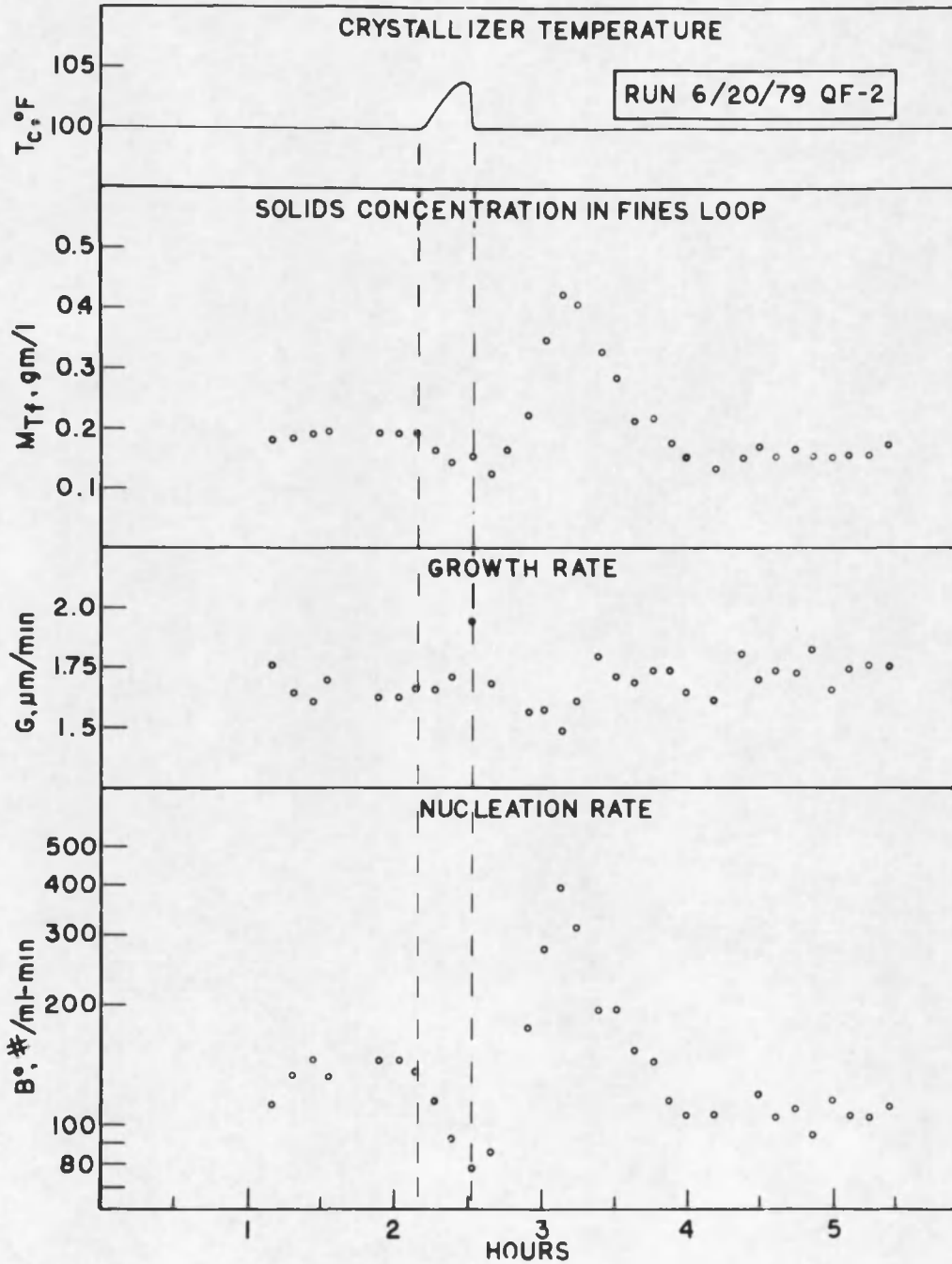


Figure 17. Response to a Temperature Upset, Run 6/20/79/QF-2.

## CHAPTER 6

### DISCUSSION AND ANALYSIS OF RESULTS

This chapter discusses the crystallizer responses and instrument performance and presents a nucleation growth rate kinetics model for the system.

#### Crystallizer Responses

##### Response at Steady State

The results from Run 5/22/79/SS-1 shown in Figure 7 illustrate on-line measurement of the system from start-up to an apparent steady-state condition. The fines crystal content and nucleation rate increased in the beginning and then leveled out after three hours of operation as expected. The growth rate remained relatively constant during the run. These parameters apparently reach a steady state although the run was not continued.

##### Response to Agitation Rate Decrease

The response for Run 6/13/79/RP-2 shown in Figure 8 resulted when the stirrer rate was abruptly decreased from 550 to 480 rpm after an initial steady state was attained. This rpm decrease caused a steady decline in nucleation rate to approximately 1/2 the initial steady-state value, i.e., from 650 no/min-ml to ca. 275.

Because the crystal deposition rate was unaltered and because most of the surface area is associated with the larger crystals (see Figure 18), there should be a considerable period of time (1-1/2 to 2 hr) before the reduced populations caused by reduced nucleation appreciably affects the surface area. Thus, supersaturation should remain more or less constant during this period. For a growth rate of 2  $\mu\text{m}/\text{min}$ , significant changes in area (and, hence, supersaturation) should begin to show up in about 100 minutes, i.e., when the population disturbance grows to 200  $\mu\text{m}$ . Thus, in this initial period, the growth rate and the supersaturation should be relatively unchanged from the steady-state values. Since the size range used in this study is 31 to 125  $\mu\text{m}$ , the Microtrac should not respond to the change for the time it takes (15 minutes) the new nuclei to grow to the minimum size it senses. After this initial "dead" time, there should be a period of about 50 minutes while the disturbance passes through the measured size ranges. The Microtrac measurements during this time might give erroneous results. After 70 minutes, a quasi-steady-state fines distribution should be re-established and  $B^\circ$  and G values should smooth out as is indeed shown in Figure 8.

After 1-1/2 to 2 hours, the disturbance will have grown sufficiently to start to change the surface area of the particles and thus change the supersaturation, growth rate, and nucleation rate. The test duration was not sufficient to follow these changes, although it appears an upward trend in  $B^\circ$  was developing.

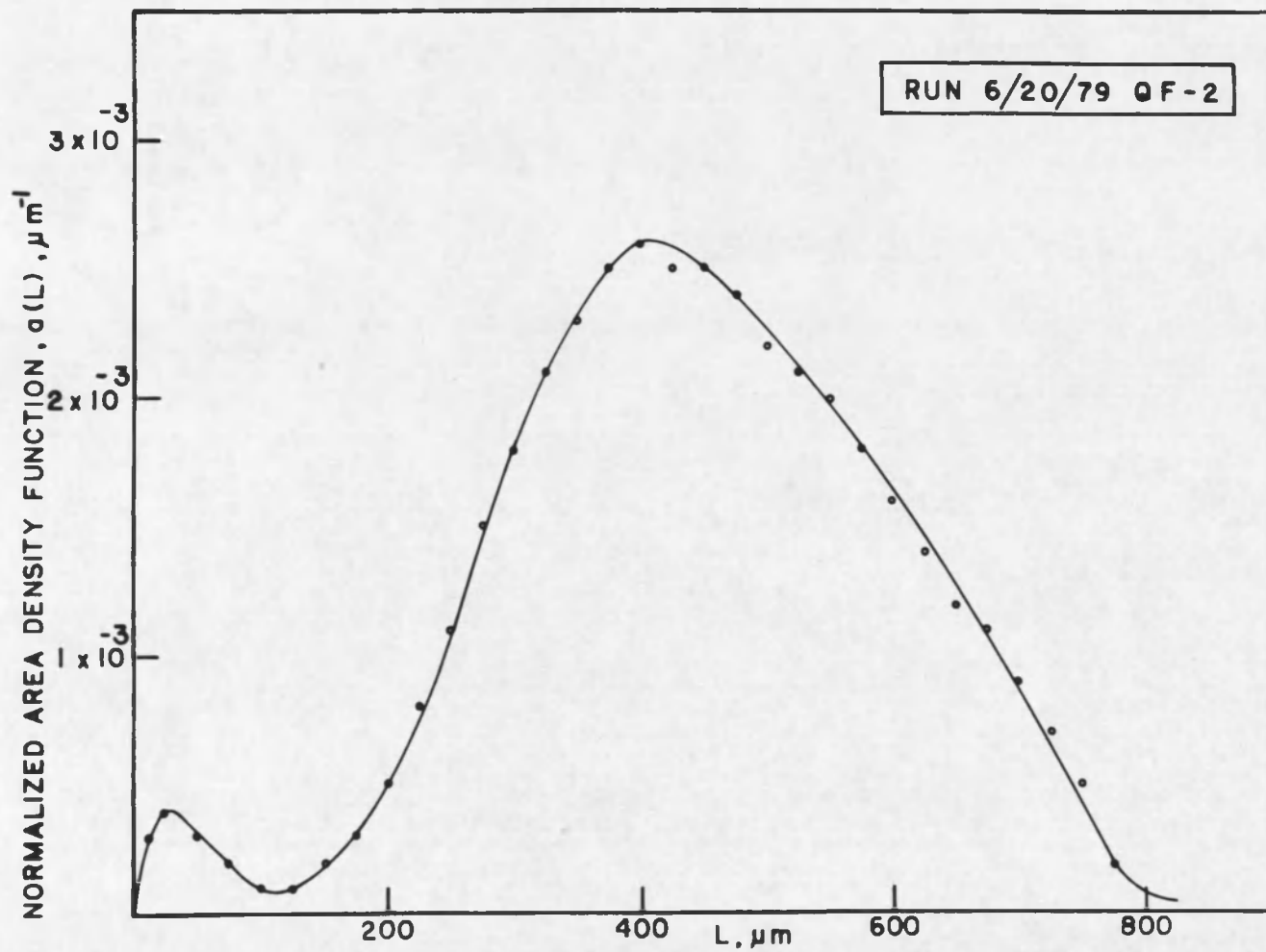


Figure 18. Distribution of Surface Area in Crystal Product Size Distribution.

### Response to Agitation Rate Increase

The results from Run 7/31/79/RP-3 are illustrated in Figure 9. A step increase in agitation was made when the system had reached steady state. This increase in agitation rate caused a steady increase in nucleation rate, which then leveled out at a quasi-steady state after 1-1/2 hours. The growth rate was relatively unchanged during this period as expected. The quasi-steady state lasted for ca. 3/4 hour. After that, the effect of increased surface area caused supersaturation to decrease and the nucleation rate started to decrease to a final steady value. The response measured in this run is better than that of Run 6/13/79/RP-2 because the test duration was longer and showed the effect of the size-induced change in supersaturation. A shorter test of a step increase in agitation rate was Run 9/5/79/RP-4 (Figure 10) which can be interpreted similarly.

### Response to Fines Rate Increase

Figure 11 shows the results for Run 5/17/79/QF-1 in which the fines removal rate was increased after a steady state was attained. The change in the fines rate decreased the fines mean residence time from 13.8 to 9.0 minutes. This new mean residence time was fed immediately to the minicomputer which resulted in the sudden apparent increase in  $G$  and  $B^\circ$ . Such a sudden change in  $G$  and  $B^\circ$  is definitely an artifact of the data reduction technique. It would take some time for the Microtrac to respond, as can be seen from the plots of  $\bar{L}_{10} = G\tau$  and  $N_T = B^\circ\tau$  which as expected, do not change for some time. The quantities  $\bar{L}_{10}$  and  $N_T$ , the population mean size and the total number concentration, are real

physical measures of the fines-crystal distribution and do not reflect artifacts in the parameters  $B^\circ$  and  $G$  resulting from the sudden mini-computer adjustment of  $\tau$ . Note, however, that the values of  $N_T$  as well as  $B^\circ$  and  $G$  begin to trend upward before the total crystal surface area can have reasonably changed to bring about an associated change in supersaturation (Figure 18). This is probably due to the accumulation changes in dissolved mass brought about by the increased rate of removal, dissolution, and recycle of dissolved fines. Thus, a step change in fines rate essentially produces a simultaneous change in the effective feed rate.

The initial increase in  $M_{Tf}$  is probably due to the increase in the classifier cut size resulting from the higher flow rate through the fines trap. With the high fines recirculation rate, these larger particles will rapidly be washed out, dissolved, and recycled, which contributes to the above-mentioned changes in solute accumulation.

Again, it will take some time before the total surface area (dominated by the larger crystals) changes sufficiently to affect the supersaturation or the growth and nucleation rates. For the first 15 minutes until the new size distribution grows to the smallest size sensed by the Microtrac, the instrument should show the "old"  $\bar{L}_{10}$  and  $N_T$  values. For the next 50 minutes, the disturbance should pass through the Microtrac sizing range causing somewhat artificial calculated values. After this period, there would be a quasi-steady state exhibited. The coarse crystal distribution would then be influenced and  $B^\circ$  and  $G$  will slowly increase and assume their final steady values. The quasi-steady period is shorter than for the case of an agitation change

because of the different fines size carried into the fines trap, causing changes in recycled dissolved solids.

#### Response to Fines Rate Decrease

In Run 6/26/79/QF-3 and Run 8/21/79/QF-4, the fines removal rates were decreased from the initial steady state. The results from these runs are shown in Figures 12 and 13.

In these two runs, the fines mean residence time was changed from 9.5 to 12.9 minutes and 10.2 to 13.2 minutes, respectively. The same interpretation as for Run 5/17/79/QF-1 applies to these runs. The sudden decrease in  $G$  and  $B^\circ$  which was calculated is an artifact due to the sudden change in  $\tau$  fed into the minicomputer. The population mean size,  $\bar{L}_{10}$ , and the total number concentration,  $N_T$ , which are real physical measures of the fines-crystal distribution, did not change during the initial period. However, the values of  $N_T$  as well as  $B^\circ$  and  $G$  began a downward trend due to the accumulation changes in dissolved mass brought about by the decreased rate of removal and recycle of dissolved fines. The initial decrease in  $M_{Tf}$  was due to the change in the classifier cut size resulting from the lower flow rate in the fines trap.

Again, after the disturbance passed through the Microtrac sizing range, a short quasi-steady-state period appeared. Finally, the coarse crystal distribution changed sufficiently to affect the super-saturation and both  $B^\circ$  and  $G$  decreased to a final steady state. The experimental results are in reasonable agreement with such a theoretical

explanation which is based on changes in solute resources and available surface area.

#### Response to Feed Rate Change

In another series of runs, the feed rate was increased or decreased after the system had reached steady state. The responses to feed rate changes are shown in Figures 14, 15, and 16. In Runs 5/15/79/QI-1 and 8/29/79/QI-4, the feed rate was increased by 40% and 25%, respectively. In Run 8/2/79/QI-3, the feed rate was decreased by 20%.

An increase (or decrease) in the feed rate causes an immediate increase (or decrease) in the crystal deposition rate and thus a rapid increase (or decrease) in supersaturation, growth rate, and nucleation rate. This will have an immediate effect on the surface area of the coarse crystals. The increase (or decrease) in the feed rate also decreases (or increases) the residence time of the fine crystals slightly. This altered value was changed within the computer and is the reason for the artificial initial increase (or decrease) in  $B^\circ$  and  $G$ . Because of the many factors changed, the dynamic behavior would be complex and is difficult to theoretically deduce. The solute resources, slurry density, crystal area, and residence time all change and interact to give the resultant  $B^\circ$  and  $G$  responses. A simple single-variable explanation as used for the RPM or fines rate change is not possible. It would be expected that growth and nucleation rate and fines crystal content would rise (or drop) reasonably quickly. This rise (or drop) would pass through the instrument size range in the first hours, giving

somewhat erroneous output values due to the non-steady fines distribution. Gradually, the surface area should build up and the growth and nucleation rate drop (or rise) to somewhat above (or below) their initial values. Run 8/29/79/QI-4 shows this phenomenon. However, Runs 8/15/79/QI-1 and 8/2/79/QI-3 were not of sufficient duration for these latter changes to be observed although a maximum (or minimum) in  $B^\circ$  and  $G$  appears to have been reached. The response measured is in reasonable agreement with this expected response.

#### Response to a Temperature Upset

Figure 17 shows the response of the crystallizer to a temperature upset. During this upset, the crystallizer temperature inadvertently rose by  $4^\circ\text{F}$  due to a cooling water failure and then suddenly cooled to the operating level as the water was restored.

While the temperature was rising the mass deposition rate decreased, causing the growth and nucleation rates to also decrease. The subsequent sudden drop in temperature caused massive nucleation which was picked up by the instrument as the particles grew into the lower counting threshold. Since the total surface area did not change much during the disturbance, the growth and nucleation rates later returned to their previous values after the particle pulse grew through the particle measuring range. An hour after the temperature was corrected, the changes had passed through the sizing range and the instrument indicated original  $G$  and  $B^\circ$  values.

### Instrument Performance

The instrument performed well in this application, requiring negligible supervision. It monitored changes in the experimental system which, in general, were in agreement with what was expected.

When a large, sudden disturbance passes through the sizing range, the method of analysis of the output produces unrealistic results due to failure of the quasi-steady-state assumption governing data regression of the measured fines. However, as more commonly happens, when the dynamic response of the crystallizer is governed by the dynamics of the coarse particles, changes are sufficiently slow for the analysis of the fines distribution to give reasonable estimates of the crystallization conditions. In practice, for control purposes, it will be necessary to distinguish between these acceptable and unrealistic outputs. For example, a weighted running average of  $B^\circ$  and  $G$  could be computed for control action and/or the output could be disregarded when the data regression correlation coefficient drops below a preset level.

The size distributions from the instrument were of good reproducibility and acceptable accuracy although only a small number of the channels contained useful information for this study. The smearing of the size distribution produces small bias errors in the estimates of  $G$  and  $B^\circ$ . For control purposes these are not important, since only deviations initiate action. For quantitative measurements, however, corrections would be necessary.

The response of the instrument would be improved if measurements could be made over a range covering smaller sizes. Large changes would

then move through the size range more rapidly and the instrument would respond faster. One way this could be done is by reducing the classifier cut size. This would also reduce the solids content, which would decrease accuracy. Some compromise is necessary and the optimal choice of cut size must be determined.

Another approach to data processing which would eliminate numerical noise in estimating and correlating population densities, but which still depends on the goodness of fit to an exponential distribution (the quasi-steady-state assumption), would be to estimate parameters using the leading moments of the fines distribution. These moments can be determined as a direct analog signal in the light scattering instrument and need not be convoluted digitally to calculate the particle distribution.

For an exponential distribution, the steady-state moments are given as:

$$m_j = j! \left( \frac{B^\circ}{G} \right) (G\tau)^{j+1} \quad [13]$$

with the recursion relationship:

$$m_j = j(G\tau) m_{j-1} \quad [14]$$

Thus, it is possible to solve directly for  $B^\circ$  and  $G$  in terms of any two of the leading moments. Thus:

$$G = \frac{m_j / m_{j-1}}{j\tau} \quad [15]$$

and

$$B^{\circ} = \left( \frac{j^j}{j!} \right) \begin{pmatrix} m_j^j \\ \frac{m_j^j - 1}{m_j} \end{pmatrix} \left( \frac{1}{\tau} \right) \quad [16]$$

It should be emphasized that this moment approach assumes an exponential population distribution over the entire size range of fines while the extrapolated population density technique illustrated in this study only utilized four points in a finite preset size range. Values of  $j$  of 3 or greater would greatly weight the results towards the larger size ranges (where most of the mass exists), while smaller values of  $j$  would weight the results towards the smaller sizes where most of the population exists. This latter case should be the more desirable except possibly for the increase in background signal which would be weighted towards the smaller sizes. A compromise between high background correction (small  $j$ ) and long response times (large  $j$ ) might be  $j=2$ , which should still give a faster response than the present analysis which considered only the larger particles. For  $j=2$ , the nucleation and growth rates would be given specifically as:

$$B^{\circ} = 2 \frac{(m_1^2/m_2)}{\tau} \quad [17]$$

$$G = \frac{m_2/m_1}{2\tau} \quad [18]$$

Use of the moments (which represent an analog integration of the laser scatter pattern) for parameter estimation might greatly reduce

the oscillatory behavior of  $B^\circ$  and  $G$  values as a particle disturbance moves through the fines size range. However, artifacts introduced by sudden changes in fines retention would still be present. This problem might be reduced by introducing changes in the fines time constant using a first-order lag of the same order as the fines response. For example, the time constant could be updated as:

$$\tau_{\text{current}} = \tau_{\text{old}} + \Delta\tau [1 - \exp(-t/\tau)] \quad [19]$$

where  $t=0$  represents the time at which a change  $\Delta\tau$  in the fines time constant is applied.

#### Nucleation Kinetics Model

In this study, steady-state nucleation rate was correlated with crystal growth rate,  $G$ , and slurry density,  $M_T$ , as indicated in equation [9]:

$$B^\circ = k_n G^i M_T^j \quad [9]$$

Data were obtained by taking average values during the steady-state period before the step change imposed in each run. The same agitation rate (RPM = 480) was used in these runs.

A summary of these experimental steady-state values is given in Table 3. The computer data output (including the entire transient period) for the runs used in the kinetic correlation is presented in Appendix C.

Table 3. Summary of Experimental Steady-State Values Used in the Determination of Kinetic Parameters.

Run	B° (no/ml-min)	G ( $\mu$ m/min)	M <sub>T</sub> (g/l)
5/15/79/QI-1	115	1.51	62
5/17/79/QF-1	112	1.44	78
6/11/79/RO-1	287	2.01	86
6/26/79/QF-3	642	2.61	109
7/31/79/RP-3	442	2.08	106
8/02/79/QI-3	511	2.02	113
8/21/79/QF-4	783	2.50	90
8/29/79/QI-4	380	1.85	95
9/05/79/RP-4	586	2.18	89

The correlation of data to this nucleation kinetics model was performed using a multiple linear regression program. This resulted in the following equation:

$$B^{\circ} = 0.88 G^{2.77} M_T^{0.91} \quad [20]$$

i.e.,  $k_n = 0.88$ ,  $i = 2.77$ , and  $j = 0.91$ . The model has an  $R^2$  value of 0.914. Figure 19 shows these experimental data fitted with the correlation line.

The resultant correlation is in good agreement with the theoretical secondary nucleation model proposed by Ness and White (1974). In their study, the effects of the number and size of crystals as well as solution supersaturation were investigated. Their model equation was:

$$B^{\circ} \propto S^{2.7} M_T^{1.3} \quad [21]$$

However, in the present study, the supersaturation was replaced by growth rate as a measure of the system driving forces.

The fit to equation [20] of the steady-state data indicates the utility of this on-line measurement technology for the realistic determination and parameter estimation of system kinetics under actual operating conditions. Such a use of this system could prove invaluable in model development of real industrial crystallizers operating with realistic plant conditions.

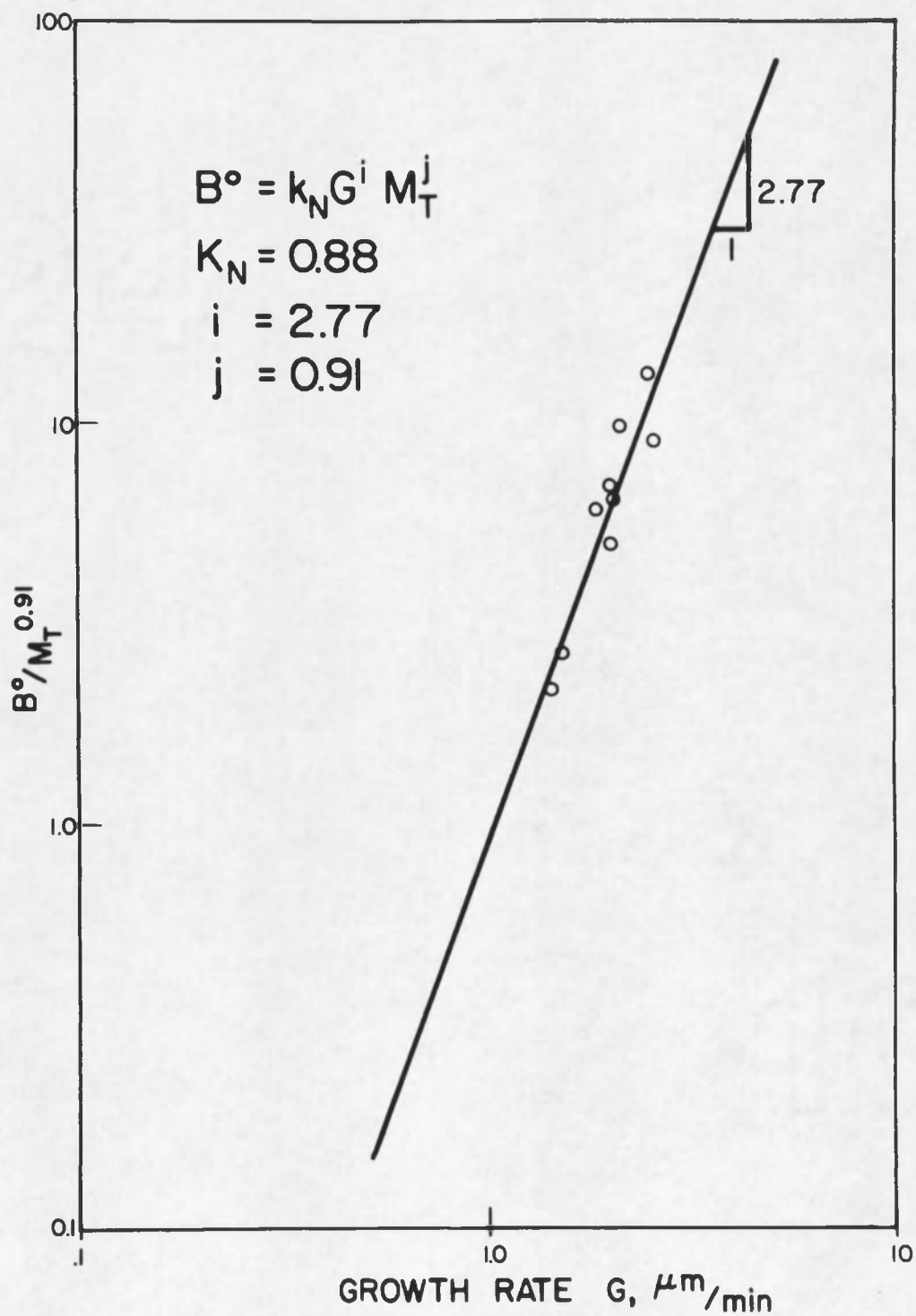


Figure 19. Nucleation Rate Correlated with Growth Rate and Slurry Density.

## CHAPTER 7

### SUMMARY AND CONCLUSIONS

1. An on-line laser light scattering particle-size analyzer was used to monitor the behavior of a continuous KCl crystallizer. The instrument was installed in the fines destruction loop.
2. Instrument output was analyzed by a real-time minicomputer front-ended with a microprocessor to calculate nucleation and growth rate in the crystallizer.
3. Calibration tests were made using garnet and KCl crystals; at particle concentrations below 1.2 g/l, instrument linearity was excellent. Initial experimental runs were made to shake down the crystallization apparatus and identify the operating ranges.
4. A number of experiments were performed to study the dynamic responses of the crystallizer. The variables studied were: agitation rate, fines removal rate, and feed rate.
5. The instrument performed well in this application, requiring negligible supervision and monitoring changes in the experimental system which were in agreement with theoretical predictions.
6. A nucleation kinetics model was developed using the steady-state experimental values. This model is in agreement with the theoretical kinetics model proposed by Ness and White (1974).

7. The on-line measurement of nucleation and growth rate could lead to feedback control schemes to stabilize a cycling crystallizer. This system has a good potential for enabling development of CSD control strategies in industrial crystallizers.

## APPENDIX A

### ON-LINE DATA REDUCTION

The Microtrac Particle Size Monitor (PSM) automation system was used to analyze the output from the Microtrac. The analysis system consisted of a SPC-16, real-time minicomputer, a KIM-1 microprocessor, and an LA-36 Decwriter. Communication between the Microtrac, LA-36, SPC-16, and the KIM-1 is described in the particle-sizer and analysis section. Table A.1 is a summary of the system commands along with a brief explanation of their functions. A listing of typical computer printout of the data reduction results is also included.

Table A.1 Summary of the System Command Options.

Option Number	Command	Description
1	PERCON	Allow the user to examine and/or change any of the permanent constants J, T, V, or L.
2	ENTER	Used to manually enter raw data values into the automation system.
3	EXAMIN	Outputs contents of the raw data buffer.
4	DELETE	Used to delete any or all current data records on disk.
5	ANALYZ	Current records in the data buffer are transformed into running natural logarithm averages and population densities are calculated and output.
6	BOUNDS	Allows bounds to be set for regression analysis and initiates the regression analysis and calculation of constants G and B°. This command must be preceded by the ANALYZ command.
7	PROCESS	Used to run commands 3, 5, and 6 without operator inputs.
8	NO OPERATOR	Allows the user to set bounds options to be used for successive runs.
9	HALT	Terminates automation system.

KIM  
0007 FD 031  
0031 AT 0

MICROTRAC FOR DATA COLLECTION SYSTEM INITIALIZED.  
AT 10:54:31 ON 02/2/77

ENTER COMMAND OR USE MICROTRAC FOR.

... ENTER OPTION

... ENTER OPTION  
1 = PERCON  
2 = ENTER  
3 = EXAMIN  
4 = DELETE  
5 = ANALYZ  
6 = BOUNDS  
7 = PROCESS  
8 = NO OPERATOR  
9 = HALT

I

... ENTER E, J, L, T, V FOR PERCON CHANGE: X TO EXIT  
E

\*\*\* PERCON CONSTANTS \*\*\*

\*\*\* J IS 14 CHANNELS  
\*\*\* TAU IS 12.8570 MINUTES  
\*\*\* VOLUME IS 0.7200E-07 CUBIC CENTIMETERS  
\*\*\* CURRENT LENGTHS FROM CHANNELS 2 TO 14

1.940	2.750	3.890	5.500	7.780
11.000	15.560	22.000	31.110	44.000
62.230	88.000	124.450	176.000	

... ENTER E, J, L, T, V FOR PERCON CHANGE: X TO EXIT  
T

\*\*\* TAU IS 12.8570 MINUTES  
... ENTER NEW VALUE  
13.636  
\*\*\* TAU IS 13.6360 MINUTES

... ENTER E, J, L, T, V FOR PERCON CHANGE: X TO EXIT  
J

\*\*\* J IS 14 CHANNELS  
... ENTER NEW VALUE  
14  
\*\*\* J IS 14 CHANNELS

... ENTER E, J, L, T, V FOR PERCON CHANGE: X TO EXIT  
X

... ENTER OPTION

```

3
### RAW MICROTRAC PSM DATA FROM THE DISK BUFFER:
REC    IV    DATA VALUES FOR CHANNEL 1 TO 13
  1    0.39    0.00    0.00    0.00    0.00    0.00    1.40    0.60    4.60    8.20    11.70    22.00    28.40    35.60
... ENTER OPTION
5
### GPL = 0.4695E+00
### FOR CHANNELS 1 TO 13 N (C=J) NUMBER / CUBIC CENTIMETERS-MICRON:
      0.4521E+06 0.1131E+06 0.2832E+05 0.7070E+04 0.1770E+04 0.6186E+03 0.4637E+02
      0.1272E+03 0.3574E+02 0.2021E+02 0.9505E+01 0.3067E+01 0.4912E+00
... ENTER OPTION
6
... ENTER ROUNDS OPTIONS
  1 = BASIC STATISTICS
  2 = ERROR TABLE
  3 = MODEL AND COEFFICIENTS
  4 = ANOVA TABLE
  5 = PRINTER PLOT
  6 = ALL OF THE ABOVE
6
### OPTIONS SELECTED
      BASIC STATISTICS
      ERROR TABLE
      MODEL AND COEFFICIENTS
      ANOVA TABLE
      PRINTER PLOT
... OK?

... LOWER BOUNDS IS 1 ENTER NEW VALUE
9
... UPPER BOUNDS IS 13 ENTER NEW VALUE
12

### LOWER BOUNDS IS 9
### UPPER BOUNDS IS 12

... OK?

```

\*\*\* RESULTS AT 5: 7:22 ON 8/ 2/77

TAU AT 13.636 MINUTES  
 VOLUME AT 0.720E-07 CURIC CENTIMETERS  
 LOWER BOUND AT CHANNEL 9  
 UPPER BOUND AT CHANNEL 12

REGRESSION EQN:

$N = 136.67 \quad \text{EXP} (-0.36232E-01 \cdot L \text{ AVE})$

WHERE: N IS IN 0/CC-MICRON L AVE IS IN MICRONS

G = 2.0240 MICRONS/MIN  
 B = 276.62 0/CC-MIN

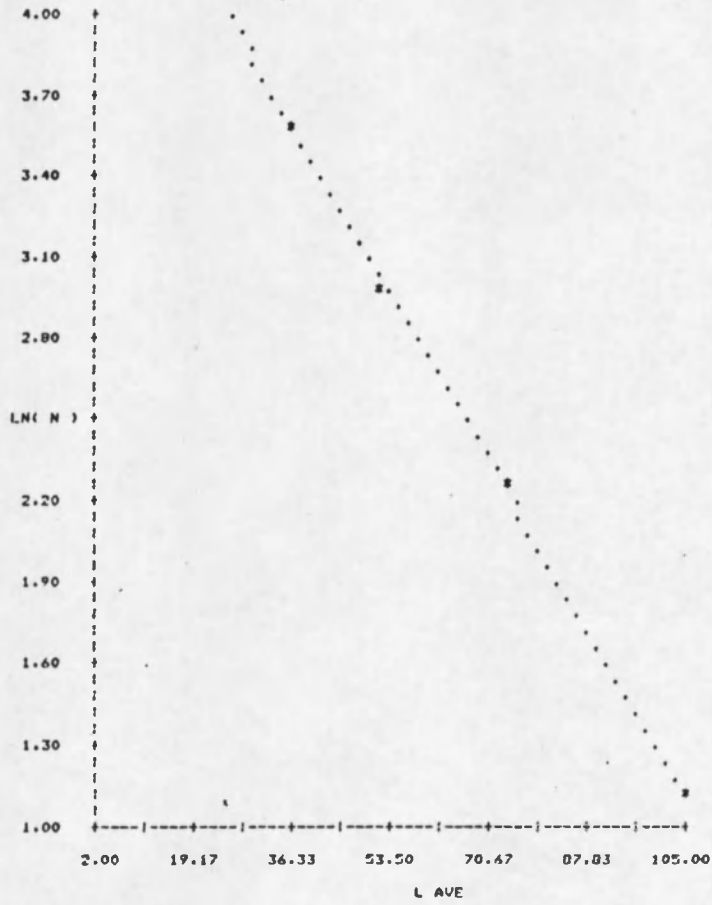
R-SQUARED = 0.99985

COEFFICIENT	VALUE	T
B0	136.67	214.99
B1	-0.36232E-01	-113.50

*** L AVE	ACTUAL N	PREDICTED N	ERROR
36.998	35.942	35.767	0.17426
52.327	20.211	20.525	-0.31323
74.002	9.5052	9.3588	0.14644
104.65	3.0675	3.0029	-0.15399E-01

ANALYSIS OF VARIANCE

SOURCE OF VARIANCE	DEGREES OF FREEDOM	SUM OF SQUARES	MEAN SQUARE	F RATIO
TOTAL	4	28.195		
MEAN	1	24.805		
TOT (CORRECTED)	3	3.3900		
REGRESSION	1	3.3895	3.3895	12881.
RESIDUAL	2	0.52626E-03	0.26313E-03	



... ENTER OPTION  
9

## APPENDIX B

### CALIBRATION AND INSTALLATION OF LIGHT SCATTERING INSTRUMENT

This appendix describes calibration of the light scattering instrument as well as details of installation and operation.

#### Calibration

##### Calibration with Particle Concentration

The calibration between the instrument dv output and the particle concentration is important for this study in order to obtain the log population density plot. The output in each size channel (which is on a relative basis) must be multiplied by this conversion factor to put on a basis of numbers per unit volume of fines liquor.

Figure B.1 shows the instrument dv values plotted against known concentrations for two samples of KCl and a garnet sample similar to the measured crystallizer distribution. It can be seen that the KCl response exhibits nonlinear behavior. The average slope of the gpl-dv response curve for the KCl sample was used to calculate  $B^\circ$  values. There are not sufficient data to say whether the shape of the particles (cubic KCl crystals with relatively flat faces vs. irregular crushed garnet) has a major effect. A similar KCl sample measured in isobutanol gave nonlinear response similar to, and to the right of, the saturated

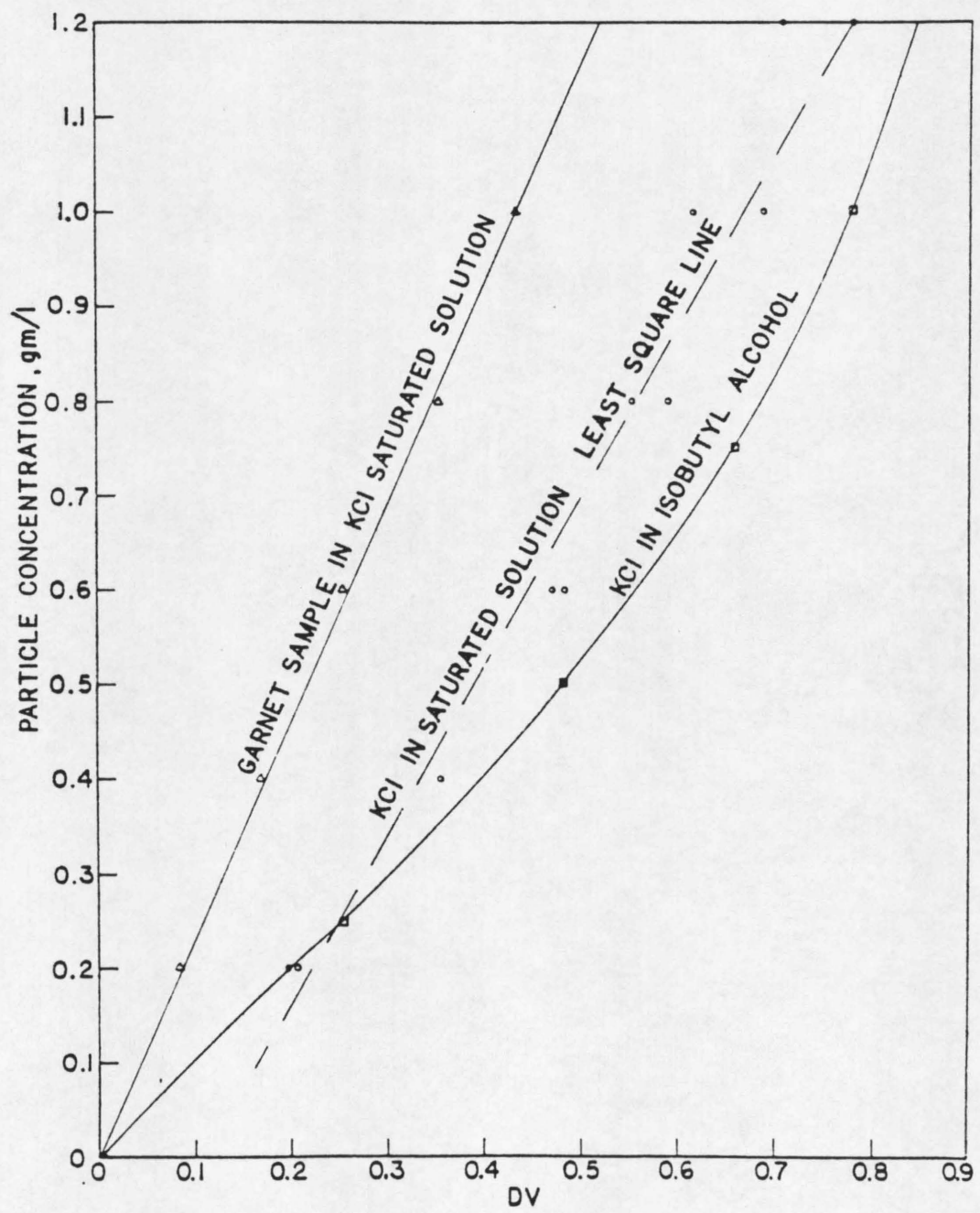


Figure B.1 Relation between Instrument Output, dv, and Particle Concentration.

KCl response. Instrument response depends on the relative difference in refractive index between solids and liquid as well as the overall CSD of the sample and must be calibrated for each application.

### Size Distribution

Table B.1 compares size distributions from the Microtrac<sup>R</sup> and a Particle Data Celloscope Particle Sizer<sup>R</sup> for a number of samples. The corresponding mass mean sizes,  $\bar{L}_{43}$ , and coefficients of variation (mass),  $CV_m$ , are listed. The Microtrac results are in reasonable agreement with the mean sizes but give a distribution with a much wider spread of sizes. This, no doubt, is related to the manipulations performed on the individual light intensities to obtain the size distribution.

This "smearing" of the size distribution may be of small consequence when no further calculations have to be performed on the size distribution. In this study, however, it has some effect when the distribution is converted to population densities. Such effect is consistent and would not interfere with the control or monitoring functions of the on-line instrument.

### Installation

Care must be taken on several aspects of installations and operation.

### Gas Bubbles

Bubbles are of large size compared to the particles and cause extensive scattering. Also, they can adhere to the optical windows, giving long-term interference. It is best if the cell is operated under

Table B.1 Comparison of Particle Size Distributions.

Sample Number	Test Material	Particle Data		Microtrac	
		$\bar{L}_{43}$ ( $\mu\text{m}$ )	$CV_m$	$\bar{L}_{43}$ ( $\mu\text{m}$ )	$CV_m$
1	KCl	111.0	0.14	112.0	0.26
2	Glass beads	24.6	0.50	21.3	0.60
3	Garnet 340# sieve	28.2	0.25	34.0	0.39
4	Garnet 170# sieve	81.7	0.14	90.5	0.38

a slight pressure to prevent air leaks and degassing from the solution. In the crystallizer, entry of gas bubbles into the fines trap caused by excessive agitation, gas bubbles in feed streams, etc., should be avoided. In sampling from the fines recirculation loop, care was taken not to sample from the top of the pipe where gas bubbles accumulate nor from the bottom where grit accumulated.

#### Crystallization within Cell

A supersaturated solution passes through the cell and thus crystallization could occur on the walls or on the cell windows, giving spurious counts. To prevent such deposition, the cell was wound with heating tape and the heating rate carefully adjusted to prevent window fouling. Overheating might cause the crystals to dissolve, though the residence time of crystals in the cell was only a few seconds.

#### Background Particles

With no particles present, the instrument still gives a reading due to scattering from the windows. There are also entrained non-crystal particles in the recirculating fines liquor. To allow for these effects, the instrument allows a background reading to be taken, which is stored and subtracted from all later readings. This makes a considerable difference in the results obtained. It is best if the background zeroing fluid is the circulating fluid with only the crystals removed.

This was readily accomplished in this study by piping the hot return liquor (after crystal dissolution) back to the cell. The background was zeroed periodically (every few hours). The instrument takes

only a minute or two to steady at the new temperature. This arrangement proved very effective, especially if, as can happen, there were large quantities of particles other than KCl circulating whose concentration changes with time. For reasonable accuracy from the instrument, it is desirable that the background be less than 30% of the particle concentration, otherwise the size distribution deteriorates because of the large subtracted background counts.

#### Particle Size and Solids Concentration

As indicated above, the solids concentration should be considerably in excess of the background for accuracy. There is also a maximum value (taken as 0.2% by volume) where multiple scattering becomes significant. The simplest way to adjust the solids concentration from the crystallizer is to alter the cut size on the fines trap by altering flow rate. If this is not feasible, a sample line hydraulic cyclone might be used either to reduce or concentrate the solids. Sample conditioning is vital to the success of the technique. For this KCl crystallizer, the cut size was in the range of 100 to 200  $\mu\text{m}$ , which gave a satisfactory solids content (up to 1.2 g/l). The background was usually less than 0.1 g/l. The maximum crystal size to which the instrument will respond is 175  $\mu\text{m}$ .

#### Maintenance

The cell windows require periodic cleaning. This was done before each series of runs. In a commercial installation, it could be at most a daily routine. The cell was manufactured of stainless steel, which

showed some corrosion in the chloride solution. This was reduced by applying a coating to the inside surfaces. All connections were of vinyl tubing.

## APPENDIX C

### EXPERIMENTAL DATA

The following tables list all of the data (both transient and steady-state) from the runs that were used to determine the nucleation kinetics model described by equation [20]. These runs encompass the major part of the work done and comprise a representative data set which is stored in this appendix as a permanent record.

Table C.1 Run 5/15/79/QI-1.

Time, t (min)	$M_{Tf}$ (g/l)	$B^\circ$ (no/ml-min)	G ( $\mu\text{m}/\text{min}$ )	$R^2$	$\bar{L}_{43}$ ( $\mu\text{m}$ )	CS ( $\text{m}^2/\text{ml}$ )	
7	0.083	65	1.66	0.989	86.7	0.135	
19	0.094	95	1.51	0.976	85.8	0.131	
23	0.086	103	1.43	0.981	82.5	0.133	
27	0.074	91	1.44	0.982	80.2	0.148	
31	0.080	67	1.67	0.978	86.2	0.109	
40	0.072	62	1.68	0.971	82.7	0.112	
48	0.086	89	1.57	0.981	82.4	0.113	
57	0.078	106	1.47	0.992	81.9	0.115	
64	0.086	109	1.48	0.989	81.8	0.106	
72	0.094	126	1.45	0.976	78.2	0.112	
83	0.103	139	1.47	0.993	79.8	0.109	
94	0.110	126	1.49	0.975	82.1	0.114	
100	0.124	153	1.44	0.969	84.8	0.100	
108	0.116	122	1.52	0.947	83.2	0.104	
135	0.096	92	1.67	0.946	94.1	0.105	
143	0.098	89	1.64	0.954	93.6	0.106	
145		(feed rate change)					
157	0.166	172	1.76	0.942	92.7	0.104	
164	0.216	254	1.71	0.973	90.1	0.093	
172	0.246	316	1.65	0.904	91.9	0.091	
180	0.308	311	1.81	0.977	92.9	0.089	
188	0.339	295	1.91	0.977	95.6	0.083	
195	0.380	380	1.82	0.968	96.5	0.081	
205	0.434	406	1.85	0.969	96.0	0.094	
213	0.455	404	1.88	0.954	98.1	0.084	
227	0.521	433	1.91	0.971	98.5	0.087	
237	0.555	472	1.90	0.954	99.7	0.080	
244	0.555	420	1.96	0.925	100.0	0.080	
252	0.587	537	1.86	0.965	98.6	0.082	
261	0.573	463	1.93	0.969	100.0	0.084	
277	0.596	549	1.83	0.935	101.0	0.078	
286	0.571	446	1.95	0.972	100.0	0.080	
299	0.535	453	1.88	0.914	100.0	0.078	
310	0.559	475	1.82	0.888	101.0	0.083	
318	0.577	463	1.89	0.934	103.0	0.078	
328	0.525	384	1.99	0.961	100.0	0.079	
340	0.522	489	1.78	0.885	101.0	0.076	
348	0.516	457	1.83	0.941	100.0	0.082	
356	0.507	433	1.88	0.944	98.1	0.092	
365	0.498	425	1.91	0.973	99.2	0.080	
375	0.516	466	1.88	0.931	99.4	0.081	

Table C.2 Run 5/17/79/QF-1.

Time, t (min)	$M_{Tf}$ (g/l)	$B^\circ$ (no/ml-min)	G ( $\mu$ m/min)	$R^2$	$\bar{L}_{10}$ ( $\mu$ m)
8	0.062	56	1.64	0.883	22.7
16	0.067	66	1.57	0.862	21.7
24	0.064	75	1.48	0.944	20.4
34	0.066	73	1.51	0.941	20.9
44	0.065	81	1.48	0.928	20.5
54	0.066	89	1.42	0.904	19.7
67	0.074	96	1.46	0.963	20.2
75	0.076	103	1.43	0.949	19.8
85	0.078	102	1.46	0.961	20.2
95	0.088	103	1.53	0.944	21.2
102	0.085	132	1.38	0.942	19.1
110	0.086	119	1.40	0.893	19.4
123		(fines removal rate change)			
124	0.110	187	2.27	0.951	20.4
133	0.079	173	2.09	0.892	18.8
143	0.076	174	2.04	0.992	18.7
153	0.075	150	2.12	0.954	19.1
162	0.077	165	2.08	0.971	18.7
170	0.073	198	1.93	0.982	17.4
186	0.079	212	1.96	0.973	17.6
200	0.085	209	2.03	0.947	18.3
210	0.093	239	2.00	0.962	18.0
220	0.107	293	1.97	0.984	17.7
235	0.117	245	2.26	0.992	20.0
248	0.123	269	2.19	0.967	19.7
255	0.127	264	2.24	0.966	20.2
263	0.124	279	2.21	0.993	19.9
270	0.133	261	2.30	0.988	20.7
278	0.142	274	2.31	0.982	20.8
290	0.155	321	2.27	0.982	20.4
297	0.166	294	2.37	0.991	21.3
310	0.187	343	2.35	0.956	21.2
318	0.209	378	2.36	0.979	21.2
327	0.214	464	2.21	0.991	20.0
337	0.220	419	2.31	0.994	20.8
345	0.228	407	2.37	0.972	21.3
357	0.239	420	2.40	0.994	21.6
370	0.267	489	2.33	0.968	21.0
383	0.279	395	2.60	0.982	23.4
390	0.297	511	2.38	0.974	21.4
398	0.286	440	2.49	0.981	22.4

Table C.2, Continued.

Time, t (min)	$M_{Tf}$ (g/l)	$B^\circ$ (no/ml-min)	G ( $\mu\text{m}/\text{min}$ )	$R^2$	$\bar{L}_{10}$ ( $\mu\text{m}$ )
406	0.303	385	2.68	0.993	24.1
416	0.312	516	2.41	0.962	21.7
424	0.335	513	2.47	0.984	22.2
431	0.330	535	2.42	0.956	21.8
440	0.341	565	2.41	0.982	21.7
450	0.358	600	2.41	0.969	21.7
457	0.383	609	2.43	0.961	21.9
467	0.382	639	2.39	0.954	21.5
474	0.389	707	2.31	0.938	20.8
482	0.396	598	2.49	0.979	22.4
496	0.417	576	2.58	0.978	23.0
505	0.436	733	2.35	0.956	21.2
520	0.435	601	2.57	0.977	23.1
528	0.449	539	2.70	0.989	24.3
534	0.440	581	2.59	0.989	23.3
541	0.423	486	2.76	0.972	24.8
549	0.429	569	2.57	0.951	23.1
560	0.409	610	2.48	0.967	22.3

Table C.3 Run 6/11/79/RP-1.

Time, t (min)	$M_{Tf}$ (g/l)	$B^\circ$ (no/ml-min)	G ( $\mu\text{m}/\text{min}$ )	$R^2$	$\bar{L}_{43}$ ( $\mu\text{m}$ )	CS ( $\text{m}^2/\text{ml}$ )
124	0.439	284	2.11	0.987	95.9	0.089
132	0.440	325	2.00	0.984	96.5	0.086
139	0.460	355	1.97	0.979	96.7	0.080
147	0.413	215	2.31	0.958	95.4	0.094
160	0.394	293	2.01	0.989	95.9	0.081
167	0.388	263	2.06	0.977	94.9	0.098
175	0.395	289	2.02	0.995	96.1	0.081
183	0.389	312	1.91	0.971	96.1	0.090
190	0.399	299	1.96	0.976	96.3	0.085
197	0.413	293	2.00	0.983	96.3	0.093
204	0.398	298	1.99	0.999	95.7	0.084
211	0.412	251	2.15	0.991	97.1	0.087
218			(RPM change)			
237	0.785	474	2.08	0.978	101.0	0.079
244	0.798	581	1.92	0.987	98.5	0.084
252	0.894	565	1.99	0.961	103.0	0.076
259	0.985	587	1.95	0.873	104.0	0.078
267	1.070	655	1.77	0.702	106.0	0.080
275	1.148	717	1.59	0.555	107.0	0.087

(particle concentration too high, experiment shut-down)

Table C.4 Run 6/26/79/QF-3.

Time, t (min)	$M_{Tf}$ (g/l)	$B^\circ$ (no/ml-min)	G ( $\mu\text{m}/\text{min}$ )	$R^2$	$\bar{L}_{43}$ ( $\mu\text{m}$ )	CS ( $\text{m}^2/\text{ml}$ )	$M_T$ (g/l)
5	0.488	580	2.50	0.990	92.5	0.092	
12	0.492	587	2.51	0.993	91.6	0.092	109
20	0.501	602	2.51	0.995	90.8	0.094	
28	0.516	619	2.50	0.994	90.8	0.094	
35	0.538	646	2.47	0.977	91.9	0.093	
43	0.561	671	2.52	0.993	91.7	0.088	
50	0.567	648	2.56	0.990	90.7	0.101	
57	0.554	679	2.49	0.981	91.8	0.091	
73	0.532	611	2.52	0.989	92.6	0.093	110
80	0.519	617	2.51	0.974	93.1	0.091	
87	0.548	517	2.79	0.999	91.4	0.100	
95	0.638	693	2.57	0.998	91.7	0.095	
102	0.636	740	2.55	0.983	94.1	0.085	108
122	0.672	667	2.68	0.986	95.4	0.087	
130	0.649	645	2.67	0.983	96.1	0.084	
138	0.601	646	2.59	0.984	94.4	0.093	
140			(fines removal rate change)				
154	0.652	605	1.81	0.986	92.8	0.088	
162	0.705	510	2.02	0.999	94.3	0.086	
172	0.738	501	2.15	0.997	97.5	0.080	
179	0.707	432	2.17	0.997	98.1	0.080	105
188	0.714	354	2.39	0.990	100.0	0.076	
195	0.710	429	2.14	0.980	100.0	0.083	
202	0.638	362	2.21	0.994	99.0	0.087	
210	0.554	337	2.13	0.993	98.8	0.085	
217	0.536	373	2.02	0.969	98.8	0.081	108
224	0.547	315	2.22	0.999	99.6	0.076	

Table C.4, Continued.

Time, t (min)	$M_{Tf}$ (g/l)	$B^\circ$ (no/ml-min)	G ( $\mu\text{m}/\text{min}$ )	$R^2$	$\bar{L}_{43}$ ( $\mu\text{m}$ )	CS ( $\text{m}^2/\text{ml}$ )	$M_T$ (g/l)
232	0.498	326	2.09	0.984	98.8	0.081	
239	0.470	321	2.03	0.976	98.0	0.090	
252	0.452	302	2.07	0.989	97.0	0.084	
260	0.390	261	2.08	0.997	96.0	0.085	
267	0.397	256	2.10	0.986	98.2	0.085	
275	0.394	261	2.05	0.989	98.2	0.081	
282	0.379	200	2.35	0.984	97.6	0.080	108
289	0.336	255	2.22	0.997	98.0	0.080	
297	0.321	224	2.02	0.983	98.9	0.080	
304	0.285	152	2.28	0.982	94.9	0.093	
311	0.399	244	2.11	0.991	101.0	0.077	
318	0.288	175	2.18	0.989	98.1	0.079	
326	0.268	178	2.07	0.986	96.7	0.082	
334	0.235	166	2.02	0.985	96.6	0.084	
341	0.228	169	1.99	0.983	96.1	0.084	107
348	0.219	149	2.06	0.991	96.6	0.081	
355	0.235	167	2.02	0.995	96.4	0.083	
363	0.214	176	1.91	0.962	94.0	0.096	
371	0.234	168	2.00	0.996	95.1	0.094	
378	0.237	153	2.12	0.997	94.5	0.088	
386	0.241	177	2.00	0.996	94.7	0.088	
393	0.230	145	2.13	0.990	95.3	0.085	
400	0.252	174	2.05	0.999	93.8	0.090	103
407	0.234	154	2.09	0.999	96.1	0.082	
415	0.230	170	2.02	0.964	96.8	0.079	

Table C.5 Run 7/31/79/RP-3.

Time, t (min)	$M_{Tf}$ (g/l)	$B^\circ$ (no/ml-min)	G ( $\mu\text{m}/\text{min}$ )	$R^2$	$\bar{L}_{43}$ ( $\mu\text{m}$ )	CS ( $\text{m}^2/\text{ml}$ )	$M_T$ (g/l)
3	0.663	462	2.05	0.987	96.3	0.082	106
10	0.683	500	2.01	0.972	97.2	0.082	
17	0.669	402	2.20	0.991	97.0	0.081	
25	0.647	400	2.16	0.999	95.8	0.090	
32	0.678	416	2.17	0.981	97.0	0.081	109
45	0.682	420	2.12	0.992	99.2	0.080	
53	0.623	433	2.04	0.978	97.4	0.080	
61	0.649	440	2.07	0.992	96.1	0.081	
68	0.645	456	2.03	0.993	97.0	0.082	113
75	0.651	426	2.09	0.991	97.1	0.081	
83	0.674	417	2.14	0.989	97.0	0.084	
90							108
98	0.709	574	1.90	0.964	95.4	0.086	
106	0.704	400	2.25	0.993	97.3	0.080	
114	0.711	405	2.26	0.979	96.4	0.082	
121	0.652	445	2.07	0.967	96.0	0.084	111
129	0.649	444	2.07	0.973	96.7	0.081	
137	0.691	484	2.05	0.989	96.6	0.081	
145	0.672	466	2.08	0.983	97.2	0.080	
152	0.680	471	2.04	0.981	97.9	0.080	
164	0.645	422	2.12	0.980	96.3	0.085	
180	0.685	499	2.03	0.981	94.4	0.088	
192	0.634	401	2.14	0.992	96.4	0.082	105
200	0.642	403	2.14	0.987	96.0	0.084	
207	0.647	454	2.02	0.989	95.2	0.087	
215	0.625	397	2.09	0.971	95.3	0.092	

Table C.5, Continued.

Time, t (min)	$M_{Tf}$ (g/l)	$B^\circ$ (no/ml-min)	G ( $\mu\text{m}/\text{min}$ )	$R^2$	$\bar{L}_{43}$ ( $\mu\text{m}$ )	CS ( $\text{m}^2/\text{ml}$ )	$M_T$ (g/l)
225	0.606	421	2.07	0.991	95.8	0.082	101
226			(RPM change)				
235	0.762	524	2.08	0.989	96.4	0.080	
243	0.798	591	1.98	0.982	95.7	0.089	
251	0.949	620	2.10	0.991	94.6	0.087	
258	1.02	767	1.98	0.971	96.3	0.080	
265	1.10	730	2.09	0.964	96.5	0.085	
273	1.19	746	2.15	0.992	97.8	0.084	
280	1.16	771	2.09	0.983	98.4	0.078	
288	1.17	627	2.32	0.997	98.7	0.080	
295	1.18	717	2.18	0.997	98.9	0.078	
303	1.15	736	2.13	0.972	99.7	0.076	105
310	1.18	677	2.23	0.981	99.7	0.078	
318	1.11	580	2.33	0.993	98.5	0.081	
325	1.06	562	2.32	0.994	99.8	0.078	
332	1.05	642	2.16	0.981	98.8	0.078	100
340	1.07	687	2.11	0.992	99.2	0.079	
347	1.05	633	2.14	0.969	99.1	0.081	
355	1.04	533	2.34	0.991	100.0	0.078	
362	1.02	439	2.58	0.992	99.4	0.083	101
370	0.996	495	2.34	0.987	99.6	0.087	
377	1.00	546	2.27	0.989	99.6	0.080	
384	0.984	498	2.35	0.998	100.0	0.080	
392	0.969	581	2.15	0.971	102.0	0.075	103
399	0.947	535	2.21	0.992	100.0	0.085	
410	0.937	589	2.10	0.985	98.9	0.086	
417	0.955	551	2.20	0.990	100.0	0.078	

Table C.5, Continued.

Time, t (min)	$M_{Tf}$ (g/l)	$B^\circ$ (no/ml-min)	G ( $\mu\text{m}/\text{min}$ )	$R^2$	$\bar{L}_{43}$ ( $\mu\text{m}$ )	CS ( $\text{m}^2/\text{ml}$ )	$M_T$ (g/l)
425	1.01	509	2.36	0.979	101.0	0.077	98
432	1.08	564	2.30	0.991	100.0	0.081	
440	1.01	494	2.40	0.999	101.0	0.075	96
447	0.976	637	2.07	0.985	100.0	0.076	
455	1.02	600	2.18	0.989	101.0	0.077	96
462	1.08	578	2.23	0.972	103.0	0.075	
470	1.10	584	2.22	0.966	102.0	0.084	96
477	1.07	580	2.24	0.992	101.0	0.089	
484	1.05	532	2.33	0.988	102.0	0.073	96
491	1.09	586	2.23	0.998	101.0	0.078	
499	1.15	707	2.07	0.952	102.0	0.076	96

Table C.6 Run 8/2/79/QI-3.

Time, t (min)	$M_{Tf}$ (g/l)	$B^\circ$ (no/ml-min)	G ( $\mu\text{m}/\text{min}$ )	$R^2$	$\bar{L}_{43}$ ( $\mu\text{m}$ )	CS ( $\text{m}^2/\text{ml}$ )	$M_T$ (g/l)	
16	0.719	496	2.05	0.994	95.5	0.086		
24	0.771	622	1.92	0.979	93.1	0.093		
31	0.743	591	1.93	0.950	95.5	0.083	112	
38	0.760	527	2.03	0.991	95.6	0.091		
46	0.711	491	2.04	0.989	94.8	0.089		
53	0.721	548	1.96	0.972	96.5	0.082		
64	0.685	558	1.92	0.982	93.9	0.087	116	
71	0.691	562	1.93	0.971	94.5	0.084		
79	0.760	498	2.10	0.994	96.1	0.088		
86	0.698	473	2.08	0.999	94.6	0.084		
93	0.719	504	2.01	0.953	97.2	0.086	109	
101	0.700	506	2.03	0.986	94.6	0.083		
109	0.676	542	1.93	0.964	93.5	0.095		
116	0.715	499	2.03	0.984	96.8	0.082		
124	0.737	504	2.06	0.995	95.2	0.090	114	
131	0.720	463	2.13	0.996	95.4	0.084		
135			(feed rate change)					
147	0.590	393	1.93	0.980	95.0	0.088		
154	0.544	327	2.03	0.999	95.7	0.083	101	
161	0.501	321	1.99	0.994	95.4	0.080		
169	0.470	276	2.02	0.999	95.0	0.085		
177	0.446	309	1.91	0.962	95.6	0.080		
185	0.478	321	1.91	0.996	95.3	0.081	101	
192	0.448	276	2.00	0.999	93.9	0.085		
200	0.455	327	1.83	0.994	94.6	0.089		
211	0.455	293	1.94	0.997	95.0	0.085	96	
218	0.448	290	1.95	0.990	95.9	0.082		

Table C.6, Continued.

Time, t (min)	$M_{Tf}$ (g/l)	$B^\circ$ (no/ml-min)	G ( $\mu\text{m}/\text{min}$ )	$R^2$	$\bar{L}_{43}$ ( $\mu\text{m}$ )	CS ( $\text{m}^2/\text{ml}$ )	$M_T$ (g/l)
225	0.458	338	1.85	0.971	96.2	0.080	
233	0.443	322	1.84	0.982	94.8	0.087	
240	0.456	331	1.83	0.972	96.4	0.083	93
247	0.453	341	1.82	0.962	95.7	0.084	
255	0.433	261	2.00	0.995	95.7	0.082	
262	0.450	328	1.85	0.991	94.7	0.084	
270	0.465	349	1.82	0.982	95.0	0.086	91
277	0.470	333	1.86	0.962	95.8	0.084	
285	0.483	340	1.96	0.979	96.8	0.081	
292	0.480	307	1.96	0.995	96.9	0.081	
300	0.507	327	1.90	0.992	97.3	0.088	89
307	0.475	308	1.93	0.995	96.3	0.083	
315	0.480	298	1.96	0.992	97.7	0.080	
322	0.448	351	1.77	0.943	97.3	0.083	
329	0.475	355	1.80	0.931	98.4	0.079	88
336	0.481	328	1.88	0.993	96.9	0.082	
343	0.483	280	2.01	0.987	97.9	0.083	
351	0.442	302	1.88	0.965	96.7	0.081	
359	0.461	315	1.85	0.969	97.3	0.088	86
366	0.466	285	1.97	0.993	98.9	0.077	
373	0.495	292	1.98	0.998	96.6	0.092	
381	0.468	251	2.04	0.993	98.4	0.082	
388	0.461	288	1.95	0.987	98.0	0.081	
396	0.488	355	1.81	0.972	98.6	0.084	84
403	0.451	296	1.90	0.991	97.4	0.083	
411	0.483	306	1.93	0.977	98.6	0.083	
418	0.448	300	1.88	0.986	97.8	0.081	

Table C.7 Run 8/21/79/QF-4.

Time, t (min)	$M_{Tf}$ (g/l)	$B^\circ$ (no/ml-min)	G ( $\mu\text{m}/\text{min}$ )	$R^2$	$\bar{L}_{43}$ ( $\mu\text{m}$ )	CS ( $\text{m}^2/\text{ml}$ )	$M_T$ (g/l)	
62	0.908	986	2.40	0.981	95.0	0.086	95	
70	0.947	855	2.51	0.996	93.4	0.096		
77	0.947	892	2.46	0.982	95.0	0.088		
92	0.884	786	2.54	0.990	93.6	0.091	91	
100	0.892	864	2.44	0.994	93.7	0.088		
107	0.903	933	2.38	0.978	93.9	0.089		
114	0.959	911	2.47	0.993	93.3	0.096		
121	0.917	928	2.41	0.991	93.5	0.088		
129	0.917	825	2.52	0.992	95.4	0.086	91	
136	0.860	805	2.46	0.954	96.5	0.084		
144	0.913	897	2.41	0.989	95.5	0.085		
151	0.890	830	2.47	0.989	96.0	0.085	90	
158	0.888	734	2.59	0.997	96.0	0.088		
165	0.856	821	2.43	0.957	95.6	0.092		
173	0.860	760	2.54	0.994	96.0	0.083		
185	0.844	774	2.49	0.998	93.9	0.094	89	
190			(fines removal rate change)					
205	0.682	562	1.83	0.980	93.7	0.089		
215	0.717	521	1.94	0.987	96.0	0.081	88	
223	0.787	534	1.97	0.985	96.8	0.084		
230	0.745	478	2.05	0.996	96.3	0.092		
238	0.734	496	1.98	0.988	96.3	0.084		
246	0.779	476	2.08	0.996	98.3	0.079	87	
254	0.711	485	1.98	0.976	97.0	0.082		
261	0.656	432	2.02	0.994	97.5	0.078		
268	0.700	407	2.11	0.993	98.9	0.078		
275	0.689	402	2.13	0.999	97.6	0.086	91	

Table C.7, Continued.

Time, t (min)	$M_{Tf}$ (g/l)	$B^\circ$ (no/ml-min)	G ( $\mu\text{m}/\text{min}$ )	$R^2$	$\bar{L}_{43}$ ( $\mu\text{m}$ )	CS ( $\text{m}^2/\text{ml}$ )	$M_T$ (g/l)
283	0.654	430	2.01	0.996	97.0	0.089	
290	0.672	388	2.15	0.997	98.9	0.076	
298	0.625	354	2.18	0.989	98.1	0.078	
306	0.597	400	2.01	0.986	97.9	0.078	
313	0.599	398	1.96	0.964	99.7	0.081	
320	0.551	355	2.03	0.998	97.0	0.080	
328	0.584	391	2.00	0.989	97.1	0.086	
335	0.544	320	2.08	0.994	97.0	0.084	84
343	0.524	299	2.14	0.991	97.8	0.086	
351	0.542	374	1.94	0.964	97.3	0.087	
358	0.539	318	2.10	0.999	97.4	0.081	
365	0.527	292	2.16	0.995	97.2	0.084	
372	0.488	325	2.01	0.999	96.5	0.079	
380	0.542	318	2.12	0.997	98.6	0.078	
387	0.498	330	2.04	0.992	96.2	0.082	
395	0.527	364	1.90	0.987	97.4	0.083	90

Table C.8 Run 8/29/79/QI-4.

Time, t (min)	$M_{Tf}$ (g/l)	$B^\circ$ (no/ml-min)	G ( $\mu\text{m}/\text{min}$ )	$R^2$	$\bar{L}_{43}$ ( $\mu\text{m}$ )	CS ( $\text{m}^2/\text{ml}$ )	$M_T$ (g/l)	
70	0.453	302	1.95	0.999	93.5	0.088		
77	0.465	330	1.87	0.978	95.6	0.082		
84	0.466	357	1.83	0.988	95.2	0.083		
92	0.491	377	1.82	0.979	94.7	0.087	95	
99	0.478	351	1.85	0.999	92.9	0.088		
106	0.486	339	1.89	0.986	95.0	0.085		
114	0.505	318	1.98	0.989	94.6	0.087		
121	0.505	372	1.85	0.998	93.6	0.087	95	
129	0.476	287	2.01	0.987	94.1	0.086		
136	0.490	358	1.84	0.993	95.1	0.084		
144	0.525	389	1.84	0.990	95.6	0.082		
151	0.507	389	1.80	0.984	95.7	0.083	95	
159	0.527	398	1.82	0.994	93.5	0.090		
165	0.534	420	1.82	0.996	93.5	0.085		
174	0.522	395	1.83	0.997	94.2	0.085		
181	0.534	409	1.82	0.983	94.7	0.087	94	
189	0.535	380	1.89	0.999	95.7	0.082		
194			(feed rate change)					
201	0.610	427	1.94	0.987	95.4	0.086		
208	0.669	476	2.01	0.992	96.2	0.083		
215	0.715	465	2.13	0.992	95.2	0.081	95	
222	0.682	523	1.95	0.986	95.5	0.086		
229	0.715	574	1.94	0.958	96.4	0.082		
236	0.687	493	2.02	0.992	95.8	0.084		
243	0.683	494	2.00	0.995	95.0	0.087		
250	0.665	544	1.91	0.986	95.3	0.085		
257	0.693	515	2.00	0.999	95.3	0.083		

Table C.8, Continued.

Time, t (min)	$M_{Tf}$ (g/l)	$B^\circ$ (no/ml-min)	G ( $\mu\text{m}/\text{min}$ )	$R^2$	$\bar{L}_{43}$ ( $\mu\text{m}$ )	CS ( $\text{m}^2/\text{ml}$ )	$M_T$ (g/l)
265	0.676	481	2.04	0.998	95.7	0.083	
272	0.680	561	1.91	0.975	95.2	0.083	105
279	0.687	472	2.07	0.999	94.6	0.084	
286	0.704	553	1.95	0.991	95.0	0.083	
293	0.711	480	2.08	0.997	96.8	0.080	106
300	0.691	535	1.95	0.977	97.0	0.080	
307	0.685	578	1.89	0.971	96.4	0.087	
315	0.680	475	2.04	0.993	96.1	0.085	
322	0.652	452	2.03	0.992	94.9	0.094	108
330	0.631	471	1.99	0.986	96.4	0.082	
337	0.631	478	1.98	0.996	95.8	0.088	
345	0.621	470	1.96	0.969	97.1	0.081	
352	0.619	499	2.11	0.996	96.0	0.081	
370	0.676	460	2.07	0.995	98.5	0.083	
378	0.647	476	1.98	0.992	95.8	0.086	
385	0.622	443	2.02	0.999	96.3	0.082	
393	0.645	413	2.11	0.997	94.9	0.090	107
400	0.639	440	2.03	0.983	96.9	0.081	

Table C.9 Run 9/5/79/RP-4.

Time, t (min)	$M_{Tf}$ (g/l)	$B^\circ$ (no/ml-min)	G ( $\mu\text{m}/\text{min}$ )	$R^2$	$\bar{L}_{43}$ ( $\mu\text{m}$ )	CS ( $\text{m}^2/\text{ml}$ )	$M_T$ (g/l)
70	0.671	678	2.00	0.995	90.2	0.097	
77	0.701	588	2.18	0.999	91.2	0.091	
84	0.709	612	2.15	0.997	91.8	0.095	
91	0.720	622	2.17	0.982	93.0	0.089	90
99	0.730	647	2.13	0.994	91.4	0.096	
106	0.752	607	2.19	0.990	94.3	0.089	
114	0.737	609	2.18	0.998	93.2	0.089	
121	0.739	650	2.11	0.991	93.5	0.093	89
129	0.717	562	2.23	0.989	95.1	0.087	
136	0.732	578	2.21	0.989	95.0	0.086	
143	0.709	617	2.14	0.996	93.2	0.091	
151	0.726	586	2.17	0.994	94.6	0.088	89
158	0.695	543	2.22	0.998	93.4	0.090	
166	0.715	625	2.13	0.980	93.1	0.091	
173	0.709	560	2.21	0.994	94.5	0.090	
181	0.705	623	2.16	0.971	94.2	0.089	89
185			(RPM change)				
195	0.700	551	2.20	0.992	94.1	0.089	
202	0.706	598	2.14	0.995	94.3	0.090	88
225	0.758	714	2.04	0.982	91.8	0.100	
232	0.819	751	2.07	0.997	93.1	0.088	
240	0.827	738	2.11	0.996	92.6	0.090	87
248	0.806	714	2.12	0.981	93.3	0.091	
255	0.852	674	2.21	0.996	93.6	0.092	
262	0.862	609	2.31	0.996	94.4	0.092	
270	0.874	775	2.10	0.984	94.0	0.096	88

Table C.9, Continued.

Time, t (min)	$M_{Tf}$ (g/l)	$B^\circ$ (no/ml-min)	G ( $\mu\text{m}/\text{min}$ )	$R^2$	$\bar{L}_{43}$ ( $\mu\text{m}$ )	CS ( $\text{m}^2/\text{ml}$ )	$M_T$ (g/l)
277	0.929	841	2.08	0.968	94.7	0.089	
285	0.878	683	2.22	0.993	94.7	0.087	
292	0.870	683	2.21	0.996	93.6	0.092	86
300	0.868	678	2.22	0.999	94.7	0.087	
307	0.846	708	2.14	0.981	94.2	0.090	
315	0.833	807	2.05	0.981	93.6	0.087	
322	0.870	674	2.22	0.995	95.5	0.085	
330	0.854	716	2.15	0.996	94.2	0.088	86

## NOMENCLATURE

$a(L)$	Normalized area density function, $(\mu\text{m})^{-1}$ .
$A_T$	Total surface area per unit volume of suspension.
$B^\circ$	Nucleation rate, no/ml-min.
$B(L)$	Particle birth function at size L, no/ml- $\mu\text{m}$ -min.
$CS$	Sample specific surface area, $\text{m}^2/\text{ml}$ .
$CV_m$	Ratio of standard deviation to mean of volume (mass) distribution.
$dv$	Uncalibrated sample volume.
$D(L)$	Particle death function at size L, no/ml- $\mu\text{m}$ -min.
$G$	Crystal growth rate, $\mu\text{m}/\text{min}$ .
$i$	Kinetic order of growth rate in power model.
$j$	Kinetic order of suspension density in power model.
$k_a$	Area shape factor.
$k_c$	Proportional control constant.
$k_n$	Secondary nucleation rate constant.
$k_v$	Volumetric shape factor.
$L$	Particle size, $\mu\text{m}$ .
$\bar{L}$	Mean particle size, $\mu\text{m}$ .
$\bar{L}_{10}$	Number-weighted mean size, $\mu\text{m}$ .
$\bar{L}_{43}$	Mass-weighted mean size, $\mu\text{m}$ .
$m_j$	$j$ -th moment of population distribution, $(\mu\text{m})^j/\text{ml}$ .
$M_T, M_{Tc}$	Solids concentration in crystallizer, gm/l.

$M_{Tf}$	Solids concentration in fines loop, gm/l.
$n$	Population density, no/ml- $\mu\text{m}$ .
$n^\circ$	Nuclei population density, no/ml- $\mu\text{m}$ .
$\bar{n}^\circ$	Steady-state nuclei population density, no/ml- $\mu\text{m}$ .
$n_i$	Inlet or outlet population density, no/ml- $\mu\text{m}$ .
$N_T$	Total number of crystals per unit volume, no/ml.
$Q_i$	Inlet or outlet volumetric flow rate, ml/min.
$Q_I$	Feed rate, ml/min.
$R$	Normalized fines destruction rate.
$\bar{R}$	Steady-state normalized fines destruction rate.
$R'$	Volume (or weight) fraction of particles with diameter greater than $x$ .
$R_s$	Critically stable fines destruction rate.
$s$	Supersaturation.
$t$	Time, min.
$T_c$	Crystallizer temperature, $^\circ\text{F}$ .
$V$	Suspension volume, ml.
$W$	Cumulative volume fraction.
$\Delta W$	Volume fraction of crystals in the size range $L$ to $L+\Delta L$ .
$x$	Equivalent sphere diameter, $\text{m}$ .
$\bar{x}$	Rosin-Rammler mean diameter, $\mu\text{m}$ .
$\tau$	Residence time, min.
$\tau_f$	Fines residence time, min.
$\rho$	Crystal density, gm/(c.c.).

## LIST OF REFERENCES

- Beckman, J. R., Ph.D. Dissertation, Department of Chemical Engineering, University of Arizona, Tucson (1976).
- Beckman, J. R., and A. D. Randolph, AICHE J., 23, 510 (1977).
- Bennett, R. C., Chem. Eng. Progrs., 58, 9 (1962).
- Brown, O. E., Cement Lime and Gravel, April (1962).
- Chang, C. T., and M. A. F. Epstein, Paper presented at the 72nd Annual AIChE Meeting, San Francisco (1979).
- Cise, M. D., Ph.D. Dissertation, Department of Chemical Engineering, University of Arizona, Tucson (1971).
- Ellis, J. K., and O. W. T. White, Control, April-June (1965).
- Farmer, W. M., Applied Optics, 11, 2603 (1972).
- Felton, P. G., and D. J. Brown, Paper presented at 6th Annual I. Chem. E. Research Meeting, U.C. London (1979).
- Gravatt, C. C., Jr., Air Pollution Control Assn. J., 23, 1035 (1973).
- Han, C. D., Paper presented at the Symposium on Selected Papers, Part I, 61st Annual Meeting, AIChE, Los Angeles (1967).
- Hulburt, H. M., and D. G. Stefango, CEP Symp. Series, 5, 50 (1969).
- Juzaszek, P., and M. A. Larson, AICHE J., 23, 460 (1977).
- Leer, B. G. M., A. Konig, and E. J. DeJong, in Industrial Crystallization, J. Mullin (ed.), Plenum Press (1976).
- Lei, S. J., R. Shinnar, and S. Katz, AICHE J., 17, 1459 (1971a).
- Lei, S. J., R. Shinnar, and S. Katz, CEP Symp. Series, 67, 129 (1971b).
- Ness, J. N., and E. T. White, Paper presented at the 77th National Meeting of AIChE, Pittsburgh (1974).

- Nuttal, H. E., Ph.D. Dissertation, Department of Chemical Engineering, University of Arizona, Tucson (1971).
- Nyvlt, J., and J. W. Mullin, Chem. Eng. Sci., 25, 131 (1970).
- Puri, A. D., M.S. Thesis, Department of Chemical Engineering, University of Arizona, Tucson (In prep.).
- Randolph, A. D., Can. J. Chem. Eng., 42, 280 (1964).
- Randolph, A. D., CEP Symp. Series (In press).
- Randolph, A. D., G. L. Beer, and J. P. Keener, AIChE J., 19, 1140 (1973).
- Randolph, A. D., J. R. Beckman, and Z. I. Kraljevich, AIChE J., 23, 500 (1977).
- Randolph, A. D., and M. D. Cise, AIChE J., 18, 798 (1972).
- Randolph, A. D., and M. A. Larson, AIChE J., 8, 639 (1962).
- Randolph, A. D., and M. A. Larson, Theory of Particular Processes, Academic Press, New York (1971).
- Randolph, A. D., and G. R. Youngquist, AIChE J., 18, 421 (1972).
- Robinson, J. V., and J. E. Roberts, Can. J. Chem. Eng., 35, 105 (1957).
- Rosonbrock, H. H., Chem. Eng. Progr., 58, 43 (1962).
- Rovang, R. D., M.S. Thesis, Department of Chemical Engineering, University of Arizona, Tucson (1978).
- Shadman, F., and A. D. Randolph, AIChE J., 24, 782 (1978).
- Sherwin, M. B., R. Shinnar, and S. Katz, AIChE J., 13, 1141 (1967).
- Sherwin, M. B., R. Shinnar, and S. Katz, CEP Symp. Series, 65, 75 (1969).
- Shields, J. P., ICI Corp. Lab., Runcorn, Cheshire, England, unpublished (1976).
- Sikdar, S. K., Ph.D. Dissertation, Department of Chemical Engineering, University of Arizona, Tucson (1975).
- Sloan, C. K., J. Phys. Chem., 59, 834 (1955).
- Timm, D. C., and G. Gupta, Paper presented at the 63rd Annual AIChE Meeting, Chicago (1970).

Weiss, E. L., and H. N. Frock, Power Technol., Summer (1976).

Wertheimer, A. L., and W. L. Wilcock, Applied Optics, 15, 1616 (1976).

Wims, A. M., and M. E. Myers, Jr., J. Coll. Interface Sci., 39, 447  
(1972).

